https://dx.doi.org/10.1016/j.ijsolstr.2018.12.017

An elastoplastic model for gap-graded soils based on homogenization theory

By

Xiusong Shi

Department of Civil and Environmental Engineering,

The Hong Kong University of Science and Technology, Hong Kong.

Email: xiusongshi@ust.hk

Jidong Zhao

Department of Civil and Environmental Engineering,

The Hong Kong University of Science and Technology, Hong Kong.

Email: jzhao@ust.hk

Jianhua Yin

Department of Civil and Environmental Engineering,

The Hong Kong Polytechnic University, Hung Hom, Kowloon, Hong Kong, China

Email: cejhyin@polyu.edu.hk

Zhijie Yu

Department of Civil and Environmental Engineering,

The Hong Kong University of Science and Technology, Hong Kong.

Email: zyuak@connect.ust.hk

December 2018

Abstract

Naturally formed soils (e.g., residual soils and deposit clays) usually show an absent range of particle size. Frequently used by geotechnical communities worldwide, such gap-graded soils can be simplified as binary mixtures composed of fine soil matrix and coarse rock aggregates. In this study, an elastoplastic model is proposed for gap-graded soils based on a volume average scheme and homogenization theory. The proposed model incorporates a structural variable to account for the evolution of the inter-granular skeleton of rock aggregates. The model is then implemented in a numerical code by the linearized integration technique proposed by Bardet and Choucair (1991). It is shown that the model can predict a wide range of variations of the overall shear responses with the increase in volume fraction of rock aggregates. An isotropic loading induces a nonuniform stress distribution in gap-graded soils, where the stress in the soil matrix is lower than that of the rock aggregates. The stress path of the matrix is approximately parallel with that of the rock aggregates during triaxial shear loading. The proposed model contains only one additional structure parameter compared with the generalized modified Cam clay model, which can be easily calibrated from the data of a conventional triaxial compression tests. Comparison between our model predictions and the experimental data from literature indicates that the propose model can well reproduce the mechanical responses of gap-graded soils within a wide range fraction of rock aggregates.

Keywords: Elastoplastic model; Gap-graded soils; Volume average scheme; Homogenization theory

1. Introduction

Natural soils are usually composed of fine-grained soil and rock aggregates with a great range gap of size distribution (Yang and Juo, 2001; Zhao *et al.*, 2007; Ueda *et al.*, 2011; Change *et al.*, 2014; Ng *et al.*, 2016; Deng *et al.*, 2017; Cui *et al.*, 2017; Xu and Coop, 2017; Yang *et al.*, 2018). Such gap-graded soils have frequently been treated by mixture theory as binary mixtures consisting of soft soil matrix and stiff rock inclusions (Vallejo, 2000; Peters and Berney, 2010; Zhou *et al.*, 2016; Shi and Yin, 2017). In arid and semi-arid areas, the fine-grained soils originate from the disintegration of parent rocks (from surface inwards) due to weathering, e.g., wetting-drying cycles or temperature oscillations. Since the disintegration is mainly a physical process, the soil matrix has the same mineral composition as the rock blocks. The soil matrix may also be a resultant of erosion and transportation of sedimentary soils from other places, followed by subsequent deposition (Chandler, 2000). However, this may probably happen in wet areas. The binary gap-graded soils are used as geotechnical structures worldwide, such as riprap, dam and high-fill subgrade (Zhao *et al.*, 2007; Vallejo, 2000; Chen and Cui, 2017). The rock fraction has a considerable influence on the workability of these geo-structures (Vallejo, 2000; Peters and Berney, 2010; Zhou *et al.*, 2016).

The mechanical behavior of gap-graded soils was documented by many previous researchers, including laboratory work (Graham *et al.*, 1989; Kumar, 1996; Yin, 1999; Vallejo, 2000; Monkul *et al.*, 2005; Monkul and Ozden, 2007; Ueda *et al.*, 2010; Shi and Yin, 2018; Shi *et al.*, 2018) and numerical simulations (González et al., 2004; Dai, 2015; Ng *et al.*, 2016; Zhou *et al.*, 2016; Shi and Herle, 2017; Wu *et al.*, 2017). Most of these works focus on the qualitative analysis of the test data, with relatively scarce theoretical work on the gap-graded soils reported. To this end, a model incorporating the coarse fraction effect is proposed here for gap-graded soils, which is further validated by reported experimental data.

2. Structure of gap-graded soils

Structure evolution with increasing volume fraction of rock aggregates

For a small volume fraction of rock inclusions, the coarse aggregates may suspend in the matrix, and the overall mechanical behavior depends on the soil matrix and the interaction between the matrix and inclusion phases. With increasing volume fraction of the aggregates, contacts between the aggregates gradually form. However, these may only be partial contacts. The inter-granular skeleton of aggregates can support a higher stress than the matrix due to the partial contacts and soil bridges between the aggregates (Jafari and Shafiee, 2004; Fei, 2016; Shi and Yin, 2017). When the volume fraction of soil matrix approximates the maximum porosity of the inclusions (loosest packing state of coarse aggregates), a continuous inter-granular skeleton forms. The corresponding fraction of the matrix is noted as ‘transition fines content’ (Monkul and Ozden, 2007). In this study, we only consider the fine content beyond the ‘transition fines content’, which corresponds to soils in intense weathering areas. An extremely small fine content (e.g., close or equal to zero) may result in macro-pores between the rock aggregates, which is beyond the scope that the mixture theory can treat.

Volume fraction of rock aggregates

Due to its dual-level configuration, it is challenging to provide an exact description of the structure of a gap-graded soil. To this end, the volume fraction concept is introduced in the subsequent analysis (see, e.g., de Boer and Ehlers, 1986; Didwania and de Boer, 1999). This concept leads to a substitute (smeared) continua with reduced physical quantities of the constituents, which can be easily incorporated into the mixture theory.

A gap-graded soil is simplified as a mixture of matrix and inclusions, with the matrix being the soft soil and the inclusions being the rock aggregates. As mentioned above, the structure transition of gap-graded soils is controlled by the volume fraction of the rock aggregates ϕ_a, provided that the rock aggregates are randomly arranged in the soil matrix. Therefore, the coarse volume fraction ϕ_a can be introduced as a bridge between the overall behavior of the mixture and that of the soft soil matrix. The compressibility of the matrix is much higher than that of the rock inclusions, thus the volume fraction of rock aggregates increases with increasing compression loading. The volume fraction of rock aggregates is hence a state dependent variable. For a given coarse mass fraction, it can be formulated as a function of the overall void ratio e and the void ratio of the soil matrix e_m:

$$\phi_a = \frac{e_m - e}{(1+e)e_m} \tag{1}$$

The void ratio of the soil matrix e_m is given as

$$e_m = \frac{\psi_a \rho_m + (1-\psi_a)\rho_a}{(1-\psi_a)\rho_a} e \tag{2}$$

where ψ_a is the dry mass fraction of rock aggregates; ρ_m and ρ_a are the particle densities of the soil matrix and the rock aggregates, respectively. Two fractions of aggregates are used in this work: the volume fraction ϕ_a and the dry mass fraction ψ_a. ϕ_a is used for homogenizing state variables of binary gap-graded soils in the sequel analysis. The dry mass fraction ψ_a is commonly adopted in laboratory tests, since it is constant during compression and shearing process. In numerical simulations, the volume fraction of aggregates depends on the stress state which is computed from the overall void ratio and the dry mass fraction of aggregates (Eqs. (1) and (2)). Note that this is not applicable for a mixture with very high coarse fractions, in which the macro-pores may exist between the rock aggregates.

Volume average stresses and strains

Due to the difference of stiffness between the two phases of a mixture, the interaction at the interface may result in a nonuniform stress (strain) field. As the essential load-carrying members of the mixture, the hard rock aggregates sustain a higher loading than that of the ductile matrix, and the loading increases with the volume fraction of the aggregates (Tandon and Weng, 1988). Correspondingly, with increasing volume fraction of the rock aggregate, the strain experienced by the matrix phase decreases, and the magnitude of stress in the matrix drops.

In the following, the focus will be placed on modeling the mechanical behavior in the frame of continuum mechanics rather than describing the microstructure of the mixture media. As suggested by Tandon and Weng (1988), the mean-field theory provides a reasonable approximation for describing the behavior of geomaterials. Using the volume fraction concept, all physical and geometric quantities can be defined in a predefined space (e.g., deformation, motion, and stress invariants). In the sequel, the stress and strain variables are approximated by the statistical average values of the real ones (de Boer, 2006). It is of convenience to use two subscripts, ‘a’ and ‘m’, to denote quantities pertaining to the rock aggregates and soil matrix, respectively. Following the volume average scheme, the overall stress tensor σ'_{ij} and overall strain tensor ε_{ij} can be expressed as

$$\sigma'_{ij}=\frac{1}{V_t}\int_{V_t}\tilde{\boldsymbol{\sigma}}'(\boldsymbol{x})\mathrm{d}V=\frac{1}{V_t}\int_{V_a}\tilde{\boldsymbol{\sigma}}'(\boldsymbol{x})\mathrm{d}V+\frac{1}{V_t}\int_{V_m}\tilde{\boldsymbol{\sigma}}'(\boldsymbol{x})\mathrm{d}V=\phi_a\sigma'_{ij,a}+(1-\phi_a)\sigma'_{ij,m} \tag{3a}$$

$$\varepsilon_{ij}=\frac{1}{V_t}\int_{V_t}\tilde{\boldsymbol{\varepsilon}}_{ij}(\boldsymbol{x})\mathrm{d}V=\frac{1}{V_t}\int_{V_a}\tilde{\boldsymbol{\varepsilon}}_{ij}(\boldsymbol{x})\mathrm{d}V+\frac{1}{V_t}\int_{V_m}\tilde{\boldsymbol{\varepsilon}}_{ij}(\boldsymbol{x})\mathrm{d}V=\phi_a\varepsilon_{ij,a}+(1-\phi_a)\varepsilon_{ij,m} \tag{3b}$$

where V_t is the representative elementary volume (REV) of gap-graded soils, $\tilde{\sigma}'(\boldsymbol{x})$ and $\tilde{\varepsilon}_{ij}(\boldsymbol{x})$ are local stress and strain over the defined REV. V_a and V_m are the volumes of the rock aggregates and soil matrix, respectively. $\sigma'_{ij,a}$, $\sigma'_{ij,m}$, $\varepsilon_{ij,a}$ and $\varepsilon_{ij,m}$ are the stress and strain variables of the two constituents. Note that the stiffness of rock aggregates is extremely high, thus, a negligible deformation can be expected within the conventional stress range, i.e.,

$\varepsilon_{ij,a} \approx 0$.

The constitutive relationship of the gap-graded soils depends on the following factors: (1) the stress-strain relationships for the two phases. The rock aggregates are extremely hard with negligible deformation, and the soil matrix shows a plastic deformation when subjected to an external loading. (2) The homogenization approaches which builds a bridge between the overall compliance (stiffness) and the respective ones of the two phases. These two factors will be addressed in the following two sections.

3. Modeling the soil matrix

Natural soil-rock mixtures usually contain a fraction of soil matrix higher than the '*transition fines content*'. In this case, the overall behavior of the mixtures depends on that of the soil matrix, partial contacts between the coarse aggregates and the interaction at the interface between the matrix and aggregates. In the absence of a continuous inter-granular skeleton, the mechanical behavior of the soil matrix provides a frame of reference for assessing the overall behavior of the gap-graded soil. It is assumed that the soil matrix follows an incremental stress-strain relationship. A numerical scheme based on the tangent homogenization is adopted to compute the overall compliance of the soil matrix (Ju and Sun, 2001).

Elastic deformation

Following the convention of classical soil mechanics, compressive stress and strain are taken as positive. An incremental elasto-plastic description is adopted for the ductile soil matrix. The incremental strains of the soil matrix $\varepsilon_{ij,m}$ is decomposed into an elastic part $\varepsilon_{ij,m}^{e}$ and a plastic part $\varepsilon_{ij,m}^{p}$:

$$\mathrm{d}\varepsilon_{ij,m} = \mathrm{d}\varepsilon_{ij,m}^{e} + \mathrm{d}\varepsilon_{ij,m}^{p} \tag{4}$$

Logarithmic volumetric strain is adopted in this study. It is assumed that the logarithmic value of the specific volume v_m changes linearly with the effective mean stress p'_m of the matrix (Butterfield, 1979) for both virgin compression and swelling curves. Following this assumption, the elastic incremental stress-strain relationship can be expressed as

$$\mathrm{d}\varepsilon^{e}_{ij,m} = \frac{1}{K_{e,m}}\left[\frac{(1+\mu_m)}{3(1-2\mu_m)}\delta_{ik}\delta_{jl} - \frac{\mu_m}{3(1-2\mu_m)}\delta_{ij}\delta_{kl}\right]\mathrm{d}\sigma'_{kl,m} \tag{5}$$

where $K_{e,m} = \dfrac{p'_m}{\kappa_m}$ is the elastic modulus, κ_m is the slope of the swelling line of the matrix in double logarithmic $\ln v_m : \ln p'_m$ relationship, μ_m is the Poisson's ratio of the soil matrix, δ_{ij}, δ_{ik}, δ_{jl} and δ_{kl} are Kronecker's symbols.

Plastic flow

The fabric of a natural gap-graded soil depends on its history of formation, and the soil may be anisotropic due to a preferred orientation of the rock aggregates during erosion, depositional and post-depositional processes (Zhou *et al*., 2017). As a preliminary investigation, only the isotropic case is considered in this study. It is widely accepted that the critical state type models (Roscoe and Burland, 1968; McDowell and Hau, 2004; Yao *et al*., 2004, 2012; Gao and Zhao, 2012, 2015, 2017; Zhao and Gao, 2016) can well reproduce the stress-strain relationship of reconstituted soils. A generalized form of the Modified Cam clay model proposed by McDowell and Hau (2004) is adopted. The yield surface for the soil matrix f_m is given as

$$f_m: \quad q_m^2 + \frac{M_m^2}{1-k_m}\left(\frac{p'_m}{p'_c}\right)^{\frac{2}{k_m}} p_c'^2 - \frac{M_m^2 p_c'^2}{1-k_m} = 0; \quad (k_m \neq 1) \tag{6}$$

where q_m is the deviatoric stress of the matrix, p'_c represents the size of the yield surface, M_m is a strength parameter corresponding to a unique critical state line in $p'_m : q$ stress plane, and k_m controls the shape of the yield surface. Note that the Critical State Line (CSL) in the compression plane changes with the shape parameter k_m.

In the sequel, the stress-strain relationship of the soil matrix will be presented following the incremental plasticity theory presented by Scott (1985) which has been adopted in plastic fractional order plasticity (Sun and Shen, 2017; Sun *et al.*, 2018). The size of the yield surface p'_c acts as a hardening variable. Consistency condition of the yield surface gives

$$\frac{\partial f_m}{\partial \sigma'_{kl}} \mathrm{d}\sigma'_{kl} + \frac{\partial f_m}{\partial p'_c} \mathrm{d}p'_c = 0 \tag{7}$$

In many critical state models, the evolution of hardening variable p'_c is assumed as a function of the plastic volumetric strain increment $\mathrm{d}\varepsilon^p_{v,m}$ (e.g., Yao *et al.*, 2009; Yao and Zhou, 2013; Hong *et al.*, 2014):

$$\mathrm{d}p'_c = \frac{\mathrm{d}p'_c}{\mathrm{d}\varepsilon^p_{v,m}} \mathrm{d}\varepsilon^p_{v,m} = \frac{p'_c}{\lambda_m - \kappa_m} \mathrm{d}\varepsilon^p_{v,m} \tag{8}$$

where λ_m is the slope of the Normal Compression Line (NCL) in double logarithmic $\ln v_m : \ln p'_m$ plot. Note that a linear relationship between $\ln v_m$ and $\ln p'_m$ is assumed for the virgin compression of the soil matrix here.

The plastic (volumetric) strain increment ($\mathrm{d}\varepsilon^p_{v,m}$ or $\mathrm{d}\varepsilon^p_{ij,m}$) of the soil matrix is related to the maximum gradient of the plastic potential surface g_m:

$$\mathrm{d}\varepsilon^p_{v,m} = \mathrm{d}\zeta_m \frac{\partial g_m}{\partial p'_m} \tag{9a}$$

$$\mathrm{d}\varepsilon^p_{ij,m} = \mathrm{d}\zeta_m \frac{\partial g_m}{\partial \sigma'_{ij,m}} \tag{9b}$$

where $\mathrm{d}\zeta_m$ is a positive plastic multiplier. Substitution of Eqs. (8) and (9a) into Eq. (7) gives

$$\mathrm{d}\zeta_m = -\frac{1}{K_{p,m}}\left(\frac{\partial g_m}{\partial \sigma'_{ij,m}}\right)^{-1} m_{ij,m} n_{kl,m} \mathrm{d}\sigma'_{kl,m} \tag{10}$$

where $K_{p,m}$ is the plastic modulus of the soil matrix, the unit vectors $m_{ij,m}$ and $n_{kl,m}$ represent the normal to the potential surface and yield surface of the matrix, respectively:

$$K_{p,m} = \frac{p'_c}{\lambda_m - \kappa_m} \frac{\dfrac{\partial f_m}{\partial p'_c}\dfrac{\partial g_m}{\partial p'_m}}{\left\|\dfrac{\partial f_m}{\partial \sigma'_{kl,m}}\right\|\left\|\dfrac{\partial g_m}{\partial \sigma'_{ij,m}}\right\|};\ n_{kl,m} = \frac{\dfrac{\partial f_m}{\partial \sigma'_{kl,m}}}{\left\|\dfrac{\partial f_m}{\partial \sigma'_{kl,m}}\right\|};\ m_{ij,m} = \frac{\dfrac{\partial g_m}{\partial \sigma'_{ij,m}}}{\left\|\dfrac{\partial g_m}{\partial \sigma'_{ij,m}}\right\|} \tag{11}$$

where $\|x_{ij}\| = \sqrt{x_{ij}x_{ij}}$. Substitution of Eqs. (5), (9b) and (10) into Eq. (4) gives

$$\mathrm{d}\varepsilon_{ij,m} = C_{ijkl,m}\mathrm{d}\sigma'_{kl,m} \tag{12a}$$

$$C_{ijkl,m} = \frac{1}{K_{e,m}}\left[\frac{(1+\mu_m)}{3(1-2\mu_m)}\delta_{ik}\delta_{jl} - \frac{\mu_m}{3(1-2\mu_m)}\delta_{ij}\delta_{kl}\right] - \frac{1}{K_{p,m}} m_{ij,m} n_{kl,m} \tag{12b}$$

4. A new homogenization approach for gap-graded soils

The majority of early homogenization studies have been developed based on linear elasticity consideration of the constituents (Eshelby, 1961; Hill, 1965; Mori and Tanaka, 1973; Lielens *et al.*, 1998). However, a gap-graded soil is not typical soils that can be described in the classical mixture theory for three-fold reasons: (1) the soil matrix in a gap-graded soil is dominantly plastic, (2) the modulus of the rock aggregates is normally much larger compared with that of the matrix, and (3) the interface between the constituents is not perfect. To this end, a new homogenization model is proposed based on mixture theory for gap-graded soils.

Effective compliance tensor

The microstructure of natural gap-graded soils can be defined by selecting a suitable REV with randomly distributed rock aggregates. The work by Tu *et al*. (2005) on mixtures with this kind of microstructure reveals that increasing the modulus of aggregates significantly improve the overall modulus for small modulus ratios (the ratio of the modulus of the aggregates to that of the matrix). Further increase of the modulus ratio brings the overall modulus to a limit state (named as ‘saturation state’ by Tu et al., 2005). Therefore, it is reasonable to relate the overall modulus of a gap-graded soil to the one of the soil matrix and the inter-granular skeleton regardless of the modulus of the rock-aggregates.

The overall modulus of a gap-graded soil increases with the volume fraction of rock aggregates, and it should meet the following two requirements: (1) for a gap-graded soil with negligible fraction of aggregates, e.g., $\phi_s \approx 0$, the overall elastic modulus K_e and plastic modulus K_p are assumed to be approximately close to the corresponding ones of the soil matrix, i.e., $K_e \approx K_{e,m}$ and $K_p \approx K_{p,m}$. (2) when the inter-granular void ratio (the ratio of the volume of inter-granular space to that of the aggregates) approaches the minimum void ratio of the rock aggregates, additional external load is mainly sustained by the inter-granular structure. Hence, the overall modulus should be much larger than that of the soil matrix.

The homogenization model proposed by Shi and Yin (2017) for the compression behavior of sand-marine clay mixtures is modified for the gap-graded soils:

$$\ln K_e = \chi \ln K_{e,m} - \ln(1-\phi_a) \tag{13a}$$

$$\ln K_p = \chi \ln K_{p,m} - \ln(1-\phi_a) \tag{13b}$$

where χ is a structure variable representing the inter-granular structure evolution given by

$$\chi = \left(\frac{\phi_a^0}{\phi_a^0 - \phi_a} \right)^{\xi} \tag{14}$$

where ξ is a structure parameter controlling the sensitivity of the structure variable on the volume fraction of rock aggregate, ϕ_a^0 is the maximum volume fraction of aggregates for pure coarse inclusions, and it corresponds to the minimum void ratio of the rock aggregates

$e_{\min}$:

$$\phi_a = \frac{1}{1+e_{\min}} \tag{15}$$

Analogous to the stress-strain relationship of the soil matrix, the overall one can be expressed as

$$\mathrm{d}\varepsilon_{ij} = \mathrm{d}\varepsilon_{ij}^{e} + \mathrm{d}\varepsilon_{ij}^{p} = C_{ijkl}\mathrm{d}\sigma'_{kl} \tag{16a}$$

$$C_{ijkl} = \frac{1}{K_e}\left[\frac{(1+\mu_m)}{3(1-2\mu_m)}\delta_{ik}\delta_{jl} - \frac{\mu_m}{3(1-2\mu_m)}\delta_{ij}\delta_{kl}\right] - \frac{1}{K_p}m_{ij}n_{kl} \tag{16b}$$

where m_{ij} and n_{kl} are unit vectors representing the normal to the potential surface and yield surface of the gap-graded soils, respectively:

$$n_{kl} = \frac{\dfrac{\partial f}{\partial \sigma'_{kl}}}{\left\|\dfrac{\partial f}{\partial \sigma'_{kl}}\right\|}; \quad m_{ij} = \frac{\dfrac{\partial g}{\partial \sigma'_{ij}}}{\left\|\dfrac{\partial g}{\partial \sigma'_{ij}}\right\|} \tag{17}$$

Stress concentration tensor

The overall compliance tensor of the gap-graded soil can be expressed as a function of the soil matrix using an incremental stress (or strain) concentration tensor. By applying the volume average scheme, the stress concentration tensor is defined as

$$\mathrm{d}\sigma'_{ij,m} = \Theta_{ijkl}\mathrm{d}\sigma'_{kl} \tag{18}$$

Considering that the deformation of the rock aggregates is negligible, the overall incremental strain of the gap-graded soils is given as

$$\mathrm{d}\varepsilon_{ij} = (1-\phi_a)\mathrm{d}\varepsilon_{ij,m} \tag{19}$$

Combination of Eqs. (12a), (16a), (18) and (19) leads to the following stress concentration tensor

$$\Theta_{ijkl} = \frac{1}{1-\phi_a} C^{-1}_{pqij,m} C_{pqkl} \tag{20}$$

Simplification of the full constitutive model

To reproduce the stress-strain curves of the gap-graded soils, one must identify the yield surface f and the plastic potential surface g in order to determine the yield direction vector n_{kl} and the plastic flow direction vector m_{ij}. In the sequel, the unit flow and loading vectors of the gap-graded soil are derived by assuming an associated flow rule.

Based on a similar form of the incremental total strain (Eq. (19)), the overall incremental plastic strain of the gap-graded soils is related to that of the soil matrix:

$$\mathrm{d}\varepsilon^p_{ij} = (1-\phi_a)\mathrm{d}\varepsilon^p_{ij,m} \tag{21}$$

The overall plastic strain increment of the gap-graded soils is proportional to the maximum gradient of the corresponding plastic potential surface g:

$$\mathrm{d}\varepsilon^p_{ij} = \mathrm{d}\zeta \frac{\partial g}{\partial \sigma'_{ij}} \tag{22}$$

Substitution of Eqs. (9b) and (22) into (21) yields the following equation:

$$\frac{\partial g}{\partial \sigma'_{ij}} = \frac{\mathrm{d}\zeta_m}{(1-\phi_a)\mathrm{d}\zeta} \frac{\partial g_m}{\partial \sigma'_{ij,m}} \tag{23}$$

where $\mathrm{d}\zeta_m$, $\mathrm{d}\zeta$, and ϕ_a are scalars. In consideration of the definitions of yield direction and flow direction vectors in Eqs. (11) and (17), it follows that

$$m_{ij} = m_{ij,m} \tag{24}$$

An associated flow rule is assumed for the gap-graded soils, i.e., the yield surface f is the same as the plastic potential surface g, so that

$$n_{ij} = m_{ij} \tag{25}$$

The compliance tensor of the gap-graded soils is represented by the following equation:

$$C_{ijkl} = \frac{1}{3K_e(1-2\mu_m)}\left[(1+\mu_m)\delta_{ik}\delta_{jl} - \mu_m\delta_{ij}\delta_{kl}\right] - \frac{1}{K_p} m_{ij,m}m_{kl,m} \tag{26}$$

5. Model parameter calibration and numerical simulations

Calibration of model parameters

The proposed elastoplastic model in the Section 4 contains seven parameters: M_m, N_m, λ_m, κ_m, μ_m, k_m, ξ. Six of them are for the constitutive model of the soil matrix, denoted by a subscript '*m*'. M_m is a strength parameter of the soil matrix, which can be calibrated from the critical state data in $p'_m : q_m$ stress plane; N_m and λ_m describe the Normal Compression Line of the soil matrix in double logarithmic $\ln v_m : \ln p'_m$ plot; κ_m corresponds to the slope of the swelling line of the clay matrix in $\ln v_m : \ln p'_m$ compression plane; μ_m is Poisson's ratio of the soil matrix, which can be determined from the initial stiffness in triaxial compression test; k_m is a shape parameter controlling the shape of the yield surface, which can be calibrated from the critical state line in $\ln v_m : \ln p'_m$ compression plane; ξ is a structure parameter describing the evolution of inter-granular skeleton with increasing volume fraction of rock aggregates.

A minimum of three conventional tests are required for the calibration of the seven model parameters: an oedometer test or isotropic compression test on the pure soil matrix, and triaxial shear tests on both the pure soil matrix and a gap-graded soil with a predefined mass fraction of the rock aggregates. N_m, λ_m and κ_m can be determined from the loading-reloading curves of an oedometer (isotropic compression test) of the soil matrix. M_m, μ_m and k_m can be calibrated from a triaxial shear test on the pure soil matrix. The structure parameter ξ is calibrated by trial and error using the data of a triaxial shear test on a gap-graded soil.

Stress integration of the constitutive model

The model presented above is a rate-type stress-strain relationship, which can be solved by the linearized integration technique proposed by Bardet and Choucair (1991). The explicit integration scheme is utilized in this work to describe the material point response of various rock-soil mixtures from literature. It can be readily implemented into finite element codes for boundary value problems, which reduces the difficulties arising from the high non-linearity of the mechanical behavior of mixture soils. The overall loading constraints for the gap-graded soils in laboratory testing conditions can be linearized into the following equation (Bardet and Choucair, 1991):

$$P_{ijk}\mathrm{d}\sigma_{jk}+Q_{ijk}\mathrm{d}\varepsilon_{jk}=\mathrm{d}Y_i \tag{27}$$

where P_{ijk} and Q_{ijk} are constant coefficients, $\mathrm{d}Y_i$ is a loading increment during a loading process. In consideration of the overall stress-strain relationship (Eq. 16), Eq. (27) becomes

$$(P_{ijk}+Q_{ipq}C_{pqjk})\mathrm{d}\sigma'_{jk}=\mathrm{d}Y_i \tag{28}$$

It is more convenient to use the stress increment of the soil matrix $\mathrm{d}\sigma'_{jk,m}$ as the principal invariants for a boundary value problem. Substitution of Eq. (18) into Eq. (28) gives

$$(P_{ist}+Q_{ipq}C_{pqst})\Theta^{-1}_{stjk}\mathrm{d}\sigma'_{jk,m}=\mathrm{d}Y_i \tag{29}$$

The numerical stress integration procedure of the proposed model is outlined as follows:

(1) Suppose an initial isotropic overall stress state $\sigma'_{jk(j\neq k)}$=0 kPa, $\sigma'_{jk(j=k)}$=10 kPa, with a uniform stress distribution $\sigma'_{kl,m}=\sigma'_{kl,a}=\sigma'_{kl}$. Under this assumption, there may be a small deviation at the initial stage of loading, which is negligible when the stress level is significantly higher than 10 kPa.

(2) Determine the stress and strain constraint tensors P_{ijk} and Q_{ijk} based on the loading

conditions in laboratory testing. The test can be either stress controlled or strain controlled, or (stress-strain) mixed controlled.

(3) For a given overall effective stress (or strain) increment at the current computation step $\mathrm{d}Y_i$, the stress increment of the soil matrix $\mathrm{d}\sigma'_{jk,m}$ is calculated.

(4) If the assumed stress state of the soil matrix $\sigma'_{jk,m}+\mathrm{d}\sigma'_{jk,m}$ is still within the yield surface (Eq. (6): $f_m(\sigma'_{jk,m}+\mathrm{d}\sigma'_{jk,m})\leq 0$), the stresses and strains are updated as

$$\sigma'_{jk,m}\leftarrow\sigma'_{jk,m}+\mathrm{d}\sigma'_{jk,m};\ \varepsilon_{jk,m}\leftarrow\varepsilon_{jk,m}+C_{jkrt,m}\mathrm{d}\sigma'_{rt,m} \tag{30a}$$

$$\sigma'_{pq}\leftarrow\sigma'_{pq}+\Theta^{-1}_{pqjk}\mathrm{d}\sigma'_{jk,m};\ \varepsilon_{pq}\leftarrow\varepsilon_{pq}+(1-\phi_s)C_{pqrt,m}\mathrm{d}\sigma'_{rt,m} \tag{30b}$$

(5) If the assumed stress state is beyond the yield surface, the stress increment is reduced so that the new stress increment $\beta\mathrm{d}\sigma'_{jk,m}$ pushes the stress state onto the yield surface, i.e., $f_m(\sigma'_{jk,m}+\beta\mathrm{d}\sigma'_{jk,m})=0$. So that the current stresses and strains are

$$\sigma'_{jk,m}\leftarrow\sigma'_{jk,m}+\beta\mathrm{d}\sigma'_{jk,m};\ \varepsilon_{jk,m}\leftarrow\varepsilon_{jk,m}+\beta C_{jkrt,m}\mathrm{d}\sigma'_{rt,m} \tag{31a}$$

$$\sigma'_{pq}\leftarrow\sigma'_{pq}+\beta\Theta^{-1}_{pqjk}\mathrm{d}\sigma'_{jk,m};\ \varepsilon_{pq}\leftarrow\varepsilon_{pq}+(1-\phi_s)\beta C_{pqrt,m}\mathrm{d}\sigma'_{rt,m} \tag{31b}$$

(6) Update the following state variables: the compliance tensor of the soil matrix $C_{jkrt,m}$, the structure variable χ, the overall compliance tensor C_{jkrt}, the stress concentration tensor Θ^{-1}_{pqjk}.

(7) Reset the loading increment $\mathrm{d}Y_i\leftarrow(1-\beta)\mathrm{d}Y_i$, and compute the stress increment $\sigma'_{jk,m}$ due to the plastic deformation (based on Eq. (29)).

(8) The stress and strain tensor are computed by using Eq. (30), and the size of the yield surface of the soil matrix p'_c is updated. Repeat steps (3)-(8) to proceed with the next round of computation until the loading is completed.

Simulations of the proposed model

Following the numerical integration procedure presented above, simulations of drained triaxial tests of gap-graded soils using the proposed model is performed in this section. The calibrated model parameters for the proposed model are given in Table 1. The shape parameter $k_m=2$ is assigned for the yield surface of the soil matrix, which is reduced to an ellipse adopted in the Modified Cam clay model. The maximum volume fraction of the pure rock aggregates is assumed to be 0.65, and the two phases (soil matrix and rock aggregates) have the same value of particle density: 2650 kg/m^3. An initial (isotropic) effective stress of 10 kPa is assumed, and the initial state of the soil matrix is assumed on the Normal Compression Line. The sample is then isotropically compressed to 200 kPa, followed by a shear process.

The simulation results of the drained triaxial test of gap-graded soils are shown in Fig.1. A small value of the structure parameter is assumed $\xi=0.05$ first, and four different rock mass fractions are considered (0.00, 0.10,0.20,0.40). It is not surprising that the sample with a higher rock fraction shows a smaller deformation, and an increase of the rock fraction improves the overall stiffness of the gap-graded soils remarkably. However, the effect of rock fraction on the overall shear strength is negligible. Note that the kinks in Fig. 1d is induced by the change of stress path (from isotropic compression to triaxial shear). To provide an insight into this phenomenon, the stress-strain curves of the soil matrix is shown in Fig. 2. It is seen that an isotropic loading leads to a non-uniform stress distribution in the gap-graded soils. The final stress (at the end of the isotropic loading process) in the soil matrix is smaller than the corresponding overall value. The stress paths of the soil matrix and the rock aggregates are almost parallel during the subsequent triaxial shear loading stage. The overall shear strength of normally consolidated mixtures is related to the critical stress state of the soil matrix and rock aggregates. A lower stress in the matrix in conjunction with a higher stress in the aggregates results in a comparable shear strength to that of the pure soil matrix.

The overall behavior of gap-graded soils with a high value of structure parameter (ξ=0.35) is presented in Fig. 3. It reveals a different coarse fraction effect from the one with a lower value of structure parameter (ξ=0.05, see Fig. 1). Both the initial stiffness and ultimate shear strength increase continuously with increasing rock fraction. This is consistent with the results of some gap-graded soils from literature (Jafari and Shafiee, 2004; Fei, 2016; Ruggeri et al., 2016). To further evaluate the performance of the proposed model, more simulations with different values of structure parameter are performed (where the dry mass fraction is assumed to be 0.40). The results are presented in Fig. 4. It indicates that overall shear strength increases as the structure parameter increases. The structure parameter is controlled by the particle shape and the particle size distribution of the coarse aggregates.

6. Validation of the proposed model

The shear strength of a gap-graded soil is affected by the volume fraction, the particle shape and particle size distribution of the rock aggregates (Jafari and Shafiee, 2004; Fei, 2016; Ruggeri et al., 2016). For some gap-graded soils the shear strength is insensitive to the volume fraction of rock aggregates until the rock particles form a continuous skeleton (Wood and Kumar, 2000). However, the shear strength of other gap-graded soils may increase continuously with increasing rock fraction (Jafari and Shafiee, 2004; Fei, 2016; Ruggeri *et al.*, 2016). Benchmark analysis in the previous section reveals that the proposed model can simulate the shear strength behavior of the above two cases by assigning different values for the structure parameter. Three gap-graded soils from literature are used to validate the proposed model: (1) the natural gap-graded soils presented by Ruggeri *et al.* (2016); (2) the Kaolin clay-gravel mixtures from Jafari and Shafiee (2004); (3) the Kaolin clay-sand mixtures (data from Wood and Kumar, 2000).

Natural gap-graded soils (*Ruggeri et al., 2016*)

The poorly graded soil investigated by Ruggeri *et al.* (2016) consists of coarse grain particles and fine grey soil matrix, with a composition of 8% clay, 27% silts, 37% sand and 28% gravel. The shape of its PSD (particle size distribution) curve shows an absence of fine sand fraction. The pure soil matrix consists of 22% clay and 78% silts, and it has a liquid limit of 30% and a plastic limit of 18%. Three different mixtures were tested based on the PSD of the coarse aggregates: (1) HTP: the first series contains aggregates smaller than 16 mm, (2) HTP10: the grain size of the second series is smaller than 2.0 mm, and (3) HTP40: the third one has a grain size finer than 0.425 mm. The mixtures were prepared by mixing the soil matrix with the coarse aggregates in dry conditions. The reconstituted sample was first consolidated in a consolidometer at a vertical stress of 200 kPa to hold the sample together, then it was further consolidated at 400 kPa followed by triaxial shear under drained conditions. Four different cases of mass fractions of the coarse aggregates (10%, 20%, 30%, and 40%) are compared with the proposed model predictions.

Kaolin clay-gravel mixtures (*Jafari and Shafiee, 2004*)

Jafari and Shafiee (2004) have performed a series of triaxial tests on clay-gravel mixtures. The soil matrix is a commercial Kaolin clay. The particle density of the Kaolin material is 2740 kg/m^3. The liquid limit and plastic limit are 69% and 31%, respectively. The gravel was retrieved from a riverbed. It consists of sub-rounded aggregates with a particle density of 2660 kg/m^3. The size of gravel particles varies within a narrow range of 4.75 mm to 6.30 mm, with an average size of 5.55mm. The minimum void ratio of the gravel material was not given by the authors, and it was assumed as 0.41 following the summary of granulometric properties of granular materials by Herle and Gudehus (1999). Three initial volume fractions of the gravel aggregates were considered: 20%, 40%, and 60%. The gravel was first mixed with dry

Kaolin clay according to designated gravel fractions. The specimens were then compacted layer by layer (ASTM1999: standard compaction test). Finally, the specimens were saturated, consolidated and compressed under undrained strain-controlled conditions. Since the Normal Compression Line of the pure Kaolin matrix was not provided by the authors, an alternative one done by Atkinson *et al.* (1987) was used for calibrating parameters, since it has approximately the same Atterberg limits as the commercial Kaolin clay used by Jafari and Shafiee (2004).

Kaolin clay-sand mixtures (*Wood and Kumar, 2000*)

The mixture tested by Wood and Kumar (2000) consists of Kaolin matrix and coarse uniform sand inclusions. The Kaolin clay has a liquid limit and plastic limit of 80% and 39%, respectively. Most of the soil particles (95%) of soil matrix are finer than 0.002 mm. The size of sand particles is more or less uniform around 2.0 mm, and the particle shape is sub-angular to sub-rounded. The maximum and minimum porosity of the coarse sand is 0.50 and 0.37, respectively. The particle densities are 2620 and 2650 kg/m^3 for kaolin and sand, respectively. First, water was added to the dry Kaolin powder to reach a desired water content of 120%. The slurry was mixed homogeneously, and then coarse sand particles were added. Finally, the sample was pre-consolidated in a consolidometer, followed by a further pre-consolidation (400 kPa), (reloading) and shearing in a triaxial cell. Three different consolidation ratios of the mixture were considered: OCR = 1.0, 1.3, and 4.0.

Model predictions on the three gap-graded mixtures

It is assumed that the mixtures have a uniform initial stress of 10 kPa, followed by an isotropic compression and a further triaxial shearing process. The model parameters for the gap-graded soils are given in Table 2, which were determined from the procedure summarized in Section 5. Note that the values of the structure parameter ξ for natural gap-graded soils are

0.57/0.60/0.63 for HTP/HTP10/HTP40, respectively. The predictions based on our model are compared against tests data for all three gap-graded mixtures are shown in Figs. 5-16.

Figs. 5-10 present a comparison of our model predictions with the experimental observations made by Ruggeri *et al.* (2016) on natural gap-graded soils. It is seen that the proposed model can well reproduce the effect of coarse fraction on the mechanical responses and volumetric deformation behavior of the tested natural gap-graded soils. The experimental results of the kaolin-clay and kaolin-gravel mixtures obtained by Jafari and Shafiee (2004) and the numerical simulations using the proposed model are presented in Figs. 11-12. The shear strength is moderately underestimated by the proposed model at the confining stress of 100 kPa, which may be attributed by the overconsolidation due to the compaction during sample preparation. The simulations are consistent with the experimental data for volume fractions of 20% and 40%, However, a difference arises between the experimental data and the simulation curves for a high fraction of aggregates (60%). This may be due to the following two reasons: (1) large pores may exist in the soil matrix or the interface between the two phases; (2) an associated flow rule is assumed for the gap-graded soils, which may be not applicable in case where the inter-granular skeleton of aggregates controls the deformation process.

Different values of shape parameter are calibrated from the data of drained triaxial tests (k_m=1.6) and from the undrained triaxial tests (k_m=2.0) (Wood and Kumar, 2000). If k_m=2.0 is adopted for all numerical simulations, comparison of predictions with the experimental data of kaolin clay-sand mixtures (Wood and Kumar, 2000) are shown in Figs. 13-16. Noticeably, the proposed model cannot well capture the overall shear stress and overall volumetric deformation in drained triaxial tests. This may be due to the fact that the shape parameter is calibrated from the undrained tests. For a better fitting of the experimental data of the pure Kaolin clay, k_m=1.6 is adopted for a further comparison for the drained case (solid lines Figs.

13 and 14). Evidently, it is seen that the difference of overall shear stress between the simulations and experimental data significantly decreases in the drain case, whereas the overall volumetric strain remains underestimated. This can be interpreted by the deficiency of the generalized modified Cam clay model which underestimates the volumetric strain of the pure kaolin matrix in drained triaxial tests.

7. Conclusions

An elastoplastic constitutive model has been proposed for gap-graded soils based on mixture theory and a volume-average homogenization scheme. Validation of the model against experimental data has been presented. A summary of the features of present model and conclusions are presented below:

(1) The effect of inter-granular skeleton is considered by incorporating a structure parameter which evolves with the volume fraction of the rock aggregates. A small value of the structure parameter yields a negligible increase of the overall shear strength. However, a higher value of structure parameter can simulate a continuous increase of overall shear strength with increasing rock fraction.

(2) Simulation of the proposed model provides insights into the mechanisms governing the evolution of inter-granular skeleton. An isotropic loading may induce a nonuniform stress distribution in gap-graded soils, where the stress in the soil matrix is lower than that of the rock aggregates. The stress paths of the phases are almost parallel during subsequent triaxial compression loading.

(3) Compared with the generalized Modified Cam clay model, the proposed model has only one additional structure parameter, which can be estimated by trial and error using the data of a triaxial compression test on gap-graded soils with a prescribed fraction of rock aggregates. The other model parameters can be calibrated from an oedometer (or isotropic compression)

test and a triaxial test on the pure soil matrix.

Test data of three different gap-graded soils from the literature are compared with the predictions of the proposed model, revealing that the proposed model can well reproduce the stress strain relationship of gap-graded soils. However, it is noteworthy that the proposed model has been targeted for binary gap-graded soils, based on the following hypotheses: The inter-granular space is fully filled with fine soil matrix. In intense weathering areas, fine content is usually beyond the minimum porosity of the pure aggregates, and no macro-pores prevail between the large aggregates (Kavvadas *et al*. 1996; Vallejo and Mawby, 2000; Zhou *et al*., 2017). Therefore, it can be simplified as binary mixtures and be treated using mixture theory. However, The macro-pores would arise in case that the volume fraction of matrix is less than the minimum porosity of pure aggregates, and the decreasing of fine fraction leave increasing macro-pores between the coarse aggregates. This kind of soils cannot be properly modelled within the mixture theory, and further efforts need to be devoted to address this issue.

Acknowledgments

This study was partially supported by the National Natural Science Foundation of China (under Grant No. 51679207) and the Research Grants Council of Hong Kong (under RGC/GRF Grant No. 16210017, TBRS Grant No. T22-603/15N and CRF Grant No. C6012-15G). The first author appreciates the funding support from VPRG Office of HKUST for his Research Assistant Professor (RAP) position. The work in this paper is also supported by a National State Key Project “973” grant (Grant No.: 2014CB047000) (sub-project No. 2014CB047001) from Ministry of Science and Technology of the People’s Republic of China and a CRF project (Grant No.: PolyU12/CRF/13E) from Research Grants Council (RGC) of Hong Kong Special Administrative Region Government (HKSARG) of China.

References

Atkinson, J. H., Richardson, D., & Robinson, P. J. (1987). Compression and extension of K_0 normally consolidated kaolin clay. *Journal of Geotechnical Engineering*, 113(12), 1468-1482.

Bardet, J. P., & Choucair, W. (1991). A linearized integration technique for incremental constitutive equations. *International Journal for Numerical and Analytical Methods in Geomechanics*, 15(1), 1-19.

Butterfield, R. (1979). A natural compression law for soils (an advance on *e*-log*p*'). *Géotechnique*, 29(4).

Chandler, R. J. (2000). The Third Glossop Lecture: Clay sediments in depositional basins: the geotechnical cycle. *Quarterly Journal of Engineering Geology and Hydrogeology*, 33(1), 7-39.

Chang, W. J., Chang, C. W., & Zeng, J. K. (2014). Liquefaction characteristics of gap-graded gravelly soils in K_0 condition. *Soil Dynamics and Earthquake Engineering*, 56, 74-85.

Chen, X. Z., Cui, Y. F. (2017). The formation of the Wulipo landslide and the resulting debris flow in Dujiangyan City, China. *Journal of Mountain Science*. 14(6), 1100-1112.

Cui, Y. F., Zhou, X. J., & Guo, C. X. (2017). Experimental study on the moving characteristics of fine grains in wide grading unconsolidated soil under heavy rainfall. *Journal of Mountain Science*, 14(3), 417-431.

Dai, B., Yang, J., & Luo, X. (2015). A numerical analysis of the shear behavior of granular soil with fines. *Particuology*, 21, 160-172.

De Boer, R. (2006). Trends in continuum mechanics of porous media (Vol. 18). *Springer Science & Business Media*.

De Boer, R., & Ehlers, W. (1986). On the problem of fluid and gas-filled elasto-plastic solids. *International journal of solids and structures*, 22(11), 1231-1242.

Deng, Y., Wu, Z., Cui, Y., Liu, S., & Wang, Q. (2017). Sand fraction effect on hydro-mechanical behavior of sand-clay mixture. *Applied Clay Science*, 135, 355-361.

Didwania, A. K., & De Boer, R. (1999). Saturated compressible and incompressible porous solids: macro-and micromechanical approaches. *Transport in porous media*, 34(1-3), 101-115.

Eshelby, J. D. (1961). Elastic inclusions and inhomogeneities. *Progress in solid mechanics*, 2(1), 89-140.

Fei, K. (2016). Experimental study of the mechanical behavior of clay-aggregate mixtures. *Engineering Geology*, 210, 1-9.

Gao, Z.W. & Zhao, J.D. (2012). Constitutive modeling of artificially cemented sand by considering fabric anisotropy. *Computers and Geotechnics*, 41, 57-69.

Gao, Z.W. & Zhao, J.D. (2015). Constitutive modeling of anisotropic sand behavior in monotonic and cyclic loading. *Journal of Engineering Mechanics*, 141(8), Article number 04015017.

Gao, Z.W. & Zhao, J.D. (2017). A non-coaxial critical-state model for sand accounting for fabric anisotropy and fabric evolution. *International Journal of Solids and Structures*, 106-107: 200-212.

González, C., Segurado, J., & LLorca, J. (2004). Numerical simulation of elasto-plastic deformation of composites: evolution of stress microfields and implications for homogenization models. *Journal of the Mechanics and Physics of Solids*, 52(7), 1573-1593.

Graham, J., Saadat, F., Gray, M. N., Dixon, D. A., & Zhang, Q. Y. (1989). Strength and volume change behaviour of a sand-bentonite mixture. Canadian Geotechnical Journal, 26(2), 292-305.

Herle, I., & Gudehus, G. (1999). Determination of parameters of a hypoplastic constitutive model from properties of grain assemblies. *Mechanics of Cohesive-frictional Materials*, 4(5), 461-486.

Hill, R. (1965). A self-consistent mechanics of composite materials. *Journal of the Mechanics and Physics of Solids*, 13(4), 213-222.

Hong, P. Y., Pereira, J. M., Cui, Y. J., Tang, A. M., Collin, F., & Li, X. L. (2014). An elastoplastic model with combined isotropic-kinematic hardening to predict the cyclic behavior of stiff clays. *Computers and Geotechnics*, 62, 193-202.

Jafari, M. K., & Shafiee, A. (2004). Mechanical behavior of compacted composite clays. *Canadian Geotechnical Journal*, 41(6), 1152-1167.

Ju, J. W., & Sun, L. Z. (2001). Effective elastoplastic behavior of metal matrix composites containing randomly located aligned spheroidal inhomogeneities. Part I: micromechanics-based formulation. *International Journal of Solids and Structures*, 38(2), 183-201.

Kavvadas, M., Hewison, L. R., Laskaratos, P. G., Seferoglou, C., & Michalis, I. (1996, April). Experiences from the construction of the Athens Metro. *In Proc. Int. Symp. Geotechical Aspects of Underground Construction in Soft Ground*. (Edited by Mair RJ and Taylor RN) (pp. 277-282).

Kumar, G. V. (1996). Some aspects of the mechanical behavior of mixtures of kaolin and coarse sand (*Doctoral dissertation, University of Glasgow*).

Lielens, G., Pirotte, P., Couniot, A., Dupret, F., & Keunings, R. (1998). Prediction of thermo-mechanical properties for compression moulded composites. *Composites Part A: Applied Science and Manufacturing*, 29(1-2), 63-70.

McDowell, G. R., & Hau, K. W. (2004). A generalised Modified Cam clay model for clay and sand incorporating kinematic hardening and bounding surface plasticity. *Granular Matter*, 6(1), 11-16.

Monkul, M. M., & Ozden, G. (2005). Effect of intergranular void ratio on one-dimensional compression behavior. In *Proceedings of International Conference on Problematic Soils*, International Society of Soil Mechanics and Geotechnical Engineering, Famagusta, Turkish Republic of Northern Cyprus (Vol. 3, pp. 1203-1209).

Monkul, M. M., & Ozden, G. (2007). Compressional behavior of clayey sand and transition fines content. *Engineering Geology*, 89(3), 195-205.

Mori, T., & Tanaka, K. (1973). Average stress in matrix and average elastic energy of materials with misfitting inclusions. *Acta metallurgica*, 21(5), 571-574.

Muir Wood, D., & Kumar, G. V. (2000). Experimental observations of behaviour of heterogeneous soils. *Mechanics of Cohesive-frictional Materials*, 5(5), 373-398.

Ng, T. T., Zhou, W., & Chang, X. L. (2016). Effect of particle shape and fine content on the behavior of binary mixture. *Journal of Engineering Mechanics*, 143(1), C4016008.

Peters, J. F., & Berney IV, E. S. (2010). Percolation threshold of sand-clay binary mixtures. *Journal of Geotechnical and Geoenvironmental Engineering*, 136(2), 310-318.

Roscoe, K. H., and Burland, J. B. (1968). On the generalized stress-strain behavior of wet clay. *Engineering plasticity*, J. Heyman and F. A. Leckie, eds., Cambridge University Press, Cambridge, UK, 535-609.

Ruggeri, P., Segato, D., Fruzzetti, V. M. E., & Scarpelli, G. (2016). Evaluating the shear strength of a natural heterogeneous soil using reconstituted mixtures. *Géotechnique*, 66(11), 941-946.

Scott, R. F. (1985). Plasticity and constitutive relations in soil mechanics (the nineteenth terzaghi lecture). *Journal of Geotechnical Engineering*, 111(5), 559-605.

Shi, X. S., & Herle, I. (2017). Numerical simulation of lumpy soils using a hypoplastic model. *Acta Geotechnica*, 12(2), 349-363.

Shi, X. S., Herle, I., & Muir Wood, D. (2018). A consolidation model for lumpy composite soils in open-pit mining. *Géotechnique*, 68(3), 189-204.

Shi, X. S., & Yin, J. (2017). Experimental and theoretical investigation on the compression behavior of sand-marine clay mixtures within homogenization framework. *Computers and Geotechnics*, 90, 14-26.

Shi, X. S., & Yin, J. (2018). Consolidation behavior for saturated sand-marine clay mixtures considering the intergranular structure evolution. *Journal of Engineering Mechanics*, 144(2), 04017166.

Sun, Y., & Shen, Y. (2017). Constitutive model of granular soils using fractional-order plastic-flow rule. *International Journal of Geomechanics*, 17(8), 04017025.

Sun, Y., Gao, Y., & Zhu, Q. (2018). Fractional order plasticity modelling of state-dependent behaviour of granular soils without using plastic potential. *International Journal of Plasticity*, 102, 53-69.

Tandon, G. P., & Weng, G. J. (1988). A theory of particle-reinforced plasticity. *Journal of Applied Mechanics*, 55(1), 126-135.

Tu, S. T., Cai, W. Z., Yin, Y., & Ling, X. (2005). Numerical simulation of saturation behavior of physical properties in composites with randomly distributed second-phase. *Journal of composite materials*, 39(7), 617-631.

Ueda, T., Matsushima, T., & Yamada, Y. (2011). Effect of particle size ratio and volume fraction on shear strength of binary granular mixture. *Granular Matter*, 13(6), 731-742.

Vallejo, L. E., & Mawby, R. (2000). Porosity influence on the shear strength of granular material-clay mixtures. *Engineering Geology*, 58(2), 125-136.

Wu, K., Rémond, S., Abriak, N., Pizette, P., Becquart, F., & Liu, S. (2017). Study of the shear behavior of binary granular materials by DEM simulations and experimental triaxial tests. *Advanced Powder Technology*, 28(9), 2198-2210.

Xu, L., & Coop, M. R. (2017). The mechanics of a saturated silty loess with a transitional mode. *Géotechnique*, 67(7), 581-596.

Yang, J., Liu, X., Guo, Y., & Liang, L. B. (2018). A unified framework for evaluating in situ state of sand with varying fines content. *Géotechnique*, 68(2),177-183.

Yang, Z. Y., & Juo, J. L. (2001). Interpretation of sieve analysis data using the box-counting method for gravelly cobbles. *Canadian geotechnical journal*, 38(6), 1201-1212.

Yao, Y. P., Hou, W., & Zhou, A. N. (2009). UH model: three-dimensional unified hardening model for overconsolidated clays. *Géotechnique*, 59(5), 451-469.

Yao, Y. P., Sun, D. A., & Luo, T. (2004). A critical state model for sands dependent on stress and density. *International Journal for Numerical and Analytical Methods in Geomechanics*, 28(4), 323-337.

Yao, Y.P., Gao, Z.W., Zhao, J.D., Wan, Z. (2012). Modified UH model: Constitutive Modeling of Overconsolidated Clays based on a Parabolic Hvorslev Envelope. *Journal of Geotechnical and Geoenvironmental Engineering*, 138(7): 860-868

Yao, Y. P., & Zhou, A. N. (2013). Non-isothermal unified hardening model: a thermo-elasto-plastic model for clays. *Géotechnique*, 63(15), 1328.

Yin, J. H. (1999). Properties and behavior of Hong Kong marine deposits with different clay contents. *Canadian Geotechnical Journal*, 36(6), 1085-1095.

Zhao, M. H., Zou, X. J., & Zou, P. X. (2007). Disintegration characteristics of red sandstone and its filling methods for highway roadbed and embankment. *Journal of Materials in Civil Engineering*, 19(5), 404-410.

Zhao, J.D. & Gao, Z.W. (2016). Unified anisotropic elasto-plastic model for sand. *Journal of Engineering Mechanics*, 142(1), Article number 04015056.

Zhou, W., Xu, K., Ma, G., Yang, L., & Chang, X. (2016). Effects of particle size ratio on the macro-and microscopic behaviors of binary mixtures at the maximum packing efficiency state. *Granular Matter*, 18(4), 81.

Zhou, Z., Yang, H., Wang, X., & Liu, B. (2017). Model development and experimental verification for permeability coefficient of soil-rock mixture. *International Journal of*

Geomechanics, 17(4), 04016106.

List of Tables

Table 1. Model parameters for benchmark analysis of the proposed model

Table 2. Model parameters for validation of the proposed model

Table 1. Model parameters for benchmark analysis of the proposed model

Parameters	M_m	N_m	λ_m	κ_m	μ_m	k_m	ξ
Value	1.4	0.6	0.05	0.01	0.22	2.0	0.00/0.05/0.20/0.35

Table 2. Model parameters for validation of the proposed model

Parameters	Natural gap-graded soils	Kaolin-gravel mixtures	Kaolin-sand mixtures
M_m	0.97	0.98	0.80
N_m	0.817	1.269	1.35
λ_m	0.056	0.089	0.085
κ_m	0.019	0.030	0.020
μ_m	0.35	0.23	0.30
k_m	2.0	1.1	2.0 (1.6)
ξ	0.57/0.60/0.63	0.07	0.05

List of Figures

Figure 1. Predictions of the drained triaxial tests with different volume fractions using the proposed model (ξ=0.05)

Figure 2. Behaviour of soil matrix in drained triaxial tests predicted by the proposed model (ξ=0.05)

Figure 3. Predictions of the drained triaxial tests with different volume fractions using the proposed model (ξ=0.35)

Figure 4. Predictions of the drained triaxial tests with different values of the structure parameter using the proposed model (ψ_a=0.40)

Figure 5. Experimental stress-strain data and numerical simulations HTP series (Natural gap-graded soils)

Figure 6. Experimental volumetric strain and numerical simulations of HTP series (Natural gap-graded soils)

Figure 7. Experimental stress-strain data and numerical simulations HTP10 series (Natural gap-graded soils)

Figure 8. Experimental volumetric strain and numerical simulations of HTP10 series (Natural gap-graded soils)

Figure 9. Experimental stress-strain data and numerical simulations HTP40 series (Natural gap-graded soils)

Figure 10. Experimental volumetric strain and numerical simulations of HTP40 series (Natural gap-graded soils)

Figure 11. Experimental stress-strain data and numerical simulations (Kaolin clay-gravel mixtures)

Figure 12. Experimental data of excess pore water pressure dissipation and numerical simulations (Kaolin clay-gravel mixtures)

Figure 13. Experimental stress-strain data and numerical simulations of drained triaxial test (Kaolin clay-sand mixtures)

Figure 14. Experimental volumetric strain and numerical simulations of drained triaxial test (Kaolin clay-sand mixtures)

Figure 15. Experimental stress-strain data and numerical simulations of undrained triaxial test (Kaolin clay-sand mixtures)

Figure 16. Experimental data of excess pore water pressure dissipation and numerical simulations of undrained triaxial test (Kaolin clay-sand mixtures)

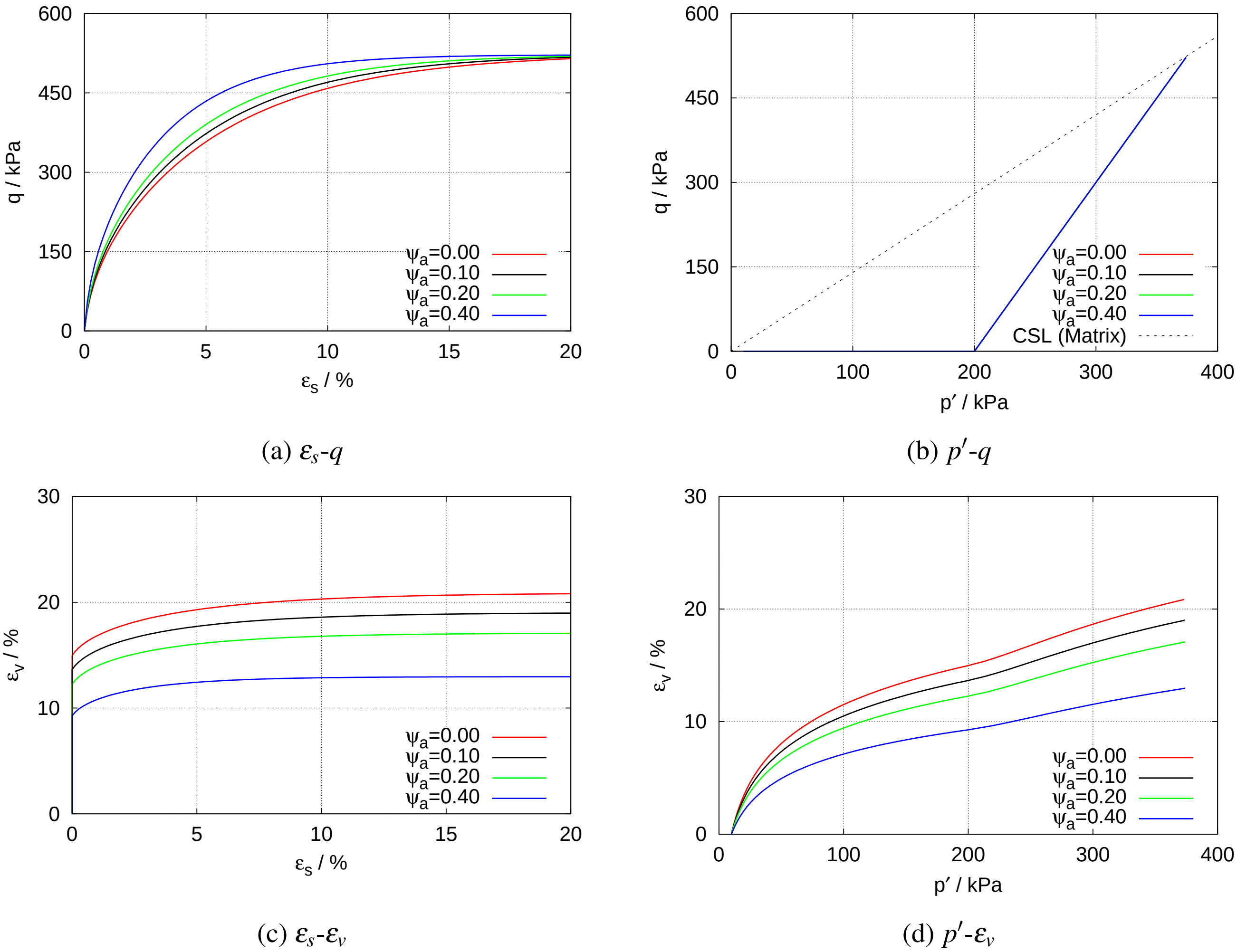

(a) ε_s-q

(b) p'-q

(c) ε_s-ε_v

(d) p'-ε_v

Figure 1: Predictions of the drained triaxial tests with different volume fractions using the proposed model (ξ=0.05)

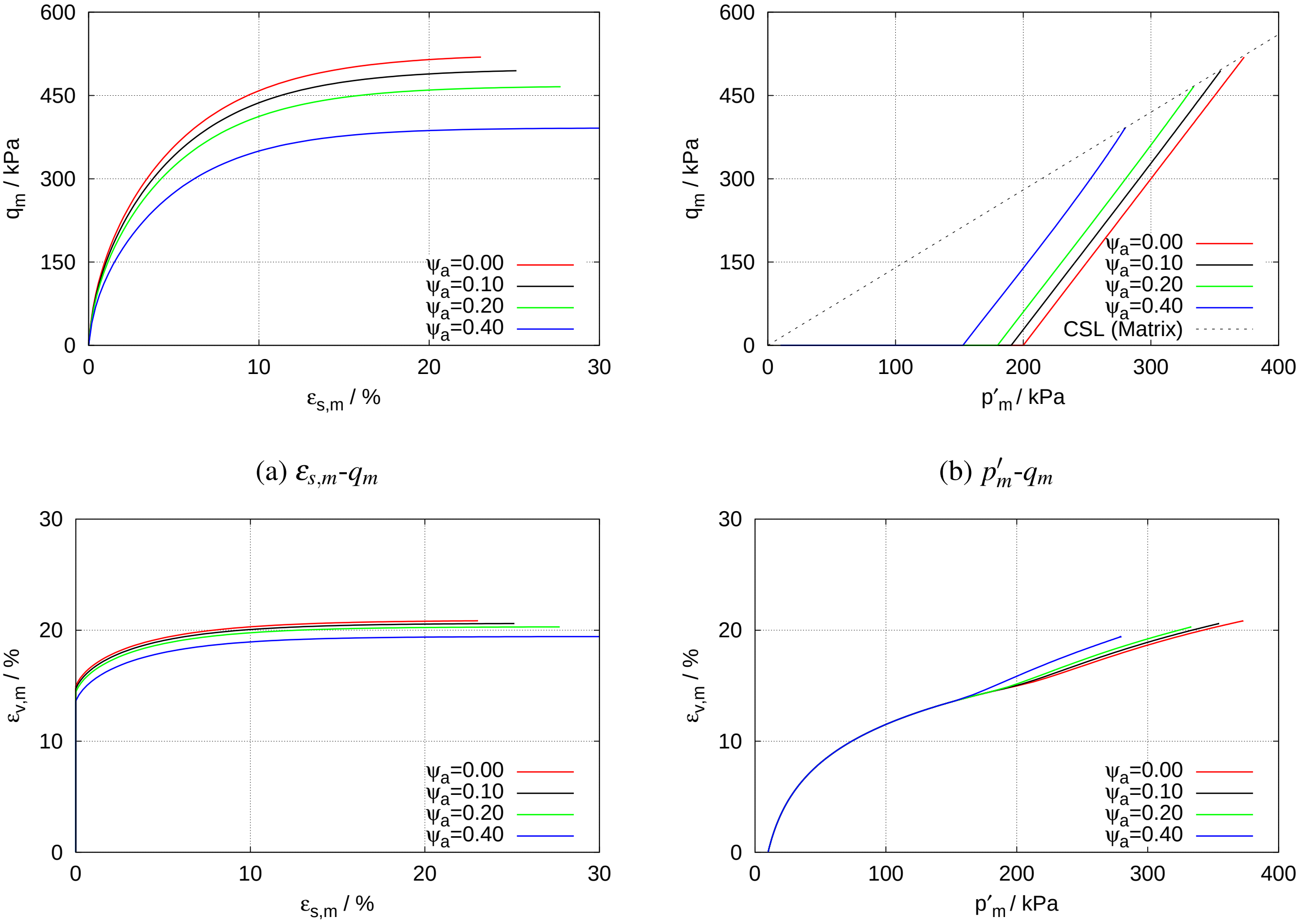

(a) $\varepsilon_{s,m}$-q_m

(b) p'_m-q_m

(c) $\varepsilon_{s,m}$-$\varepsilon_{v,m}$

(d) p'_m-$\varepsilon_{v,m}$

Figure 2: Behaviour of soil matrix in drained triaxial tests predicted by the proposed model (ξ=0.05)

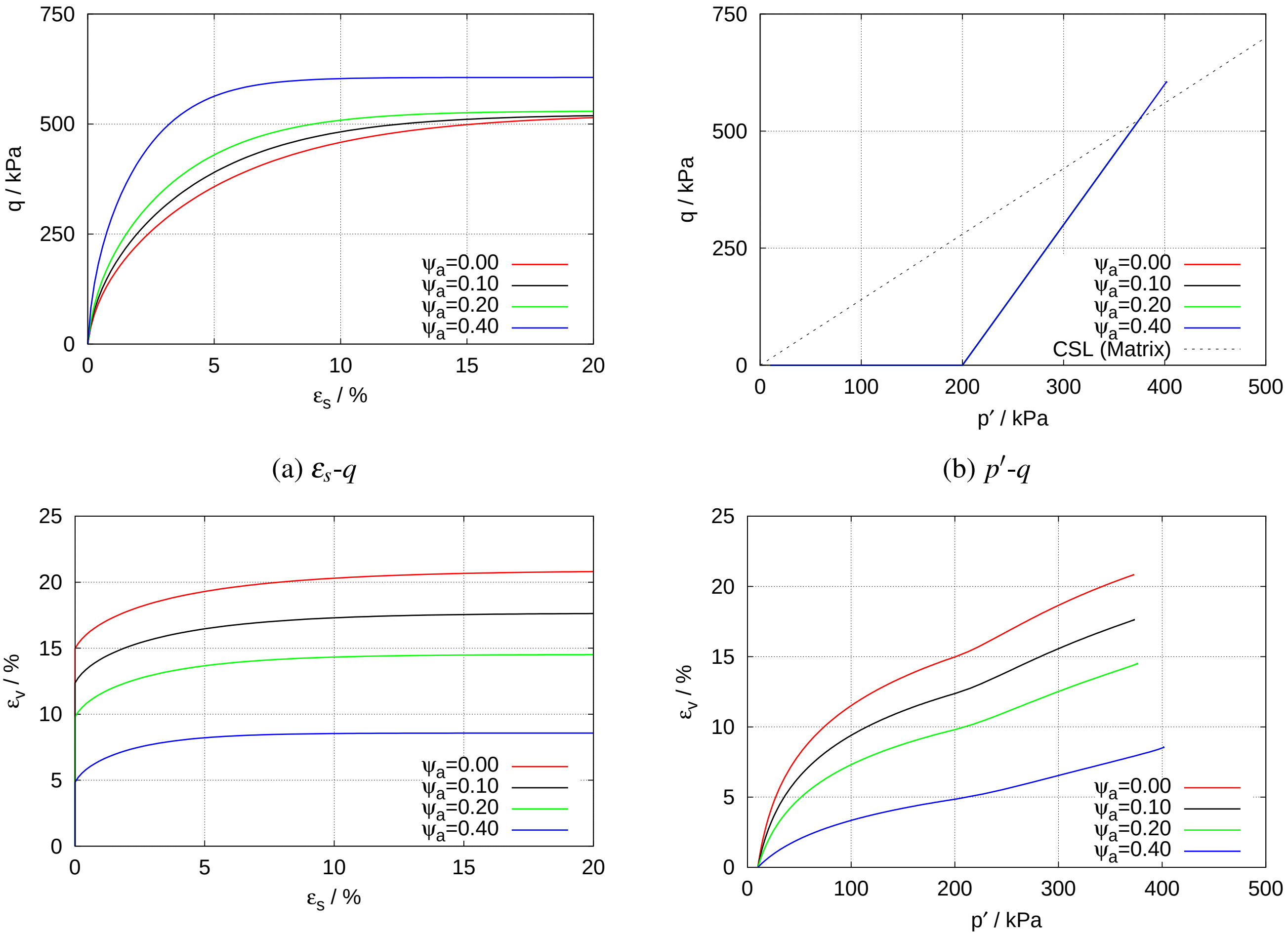

(a) ε_s-q

(b) p'-q

(c) ε_s-ε_v

(d) p'-ε_v

Figure 3: Predictions of the drained triaxial tests with different volume fractions using the proposed model (ξ=0.35)

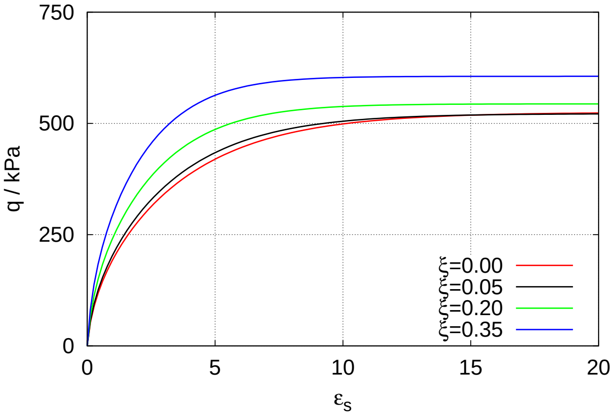

(a) ε_s-q

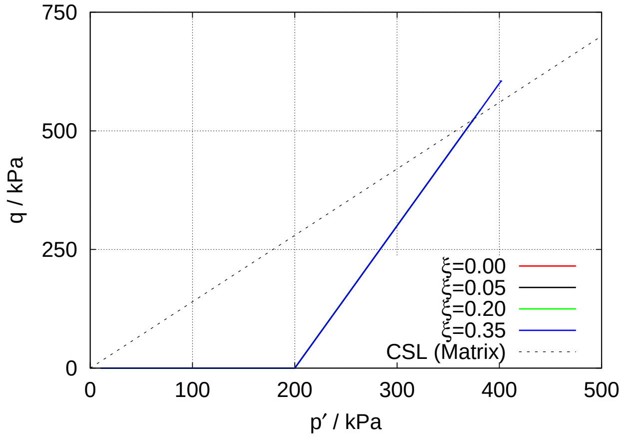

(b) p'-q

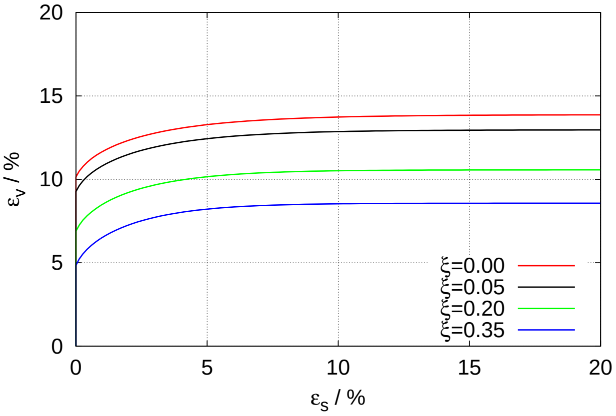

(c) ε_s-ε_v

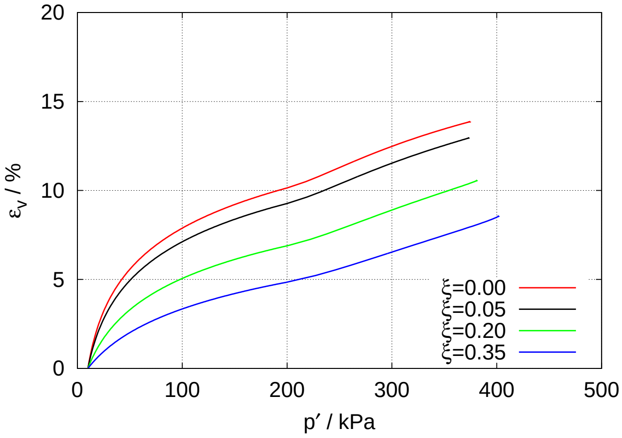

(d) p'-ε_v

Figure 4: Predictions of the drained triaxial tests with different values of the structure parameter using the proposed model (ψ_a=0.40)

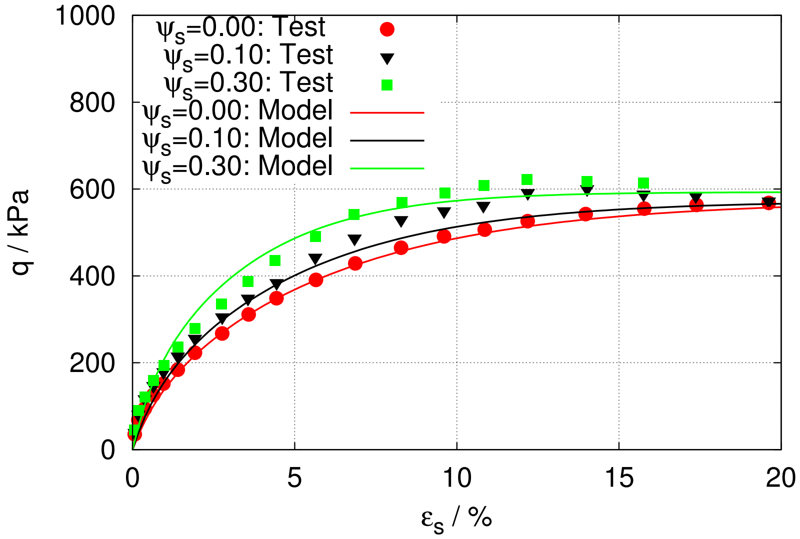

(a) ψ_a=0.10, 0.30

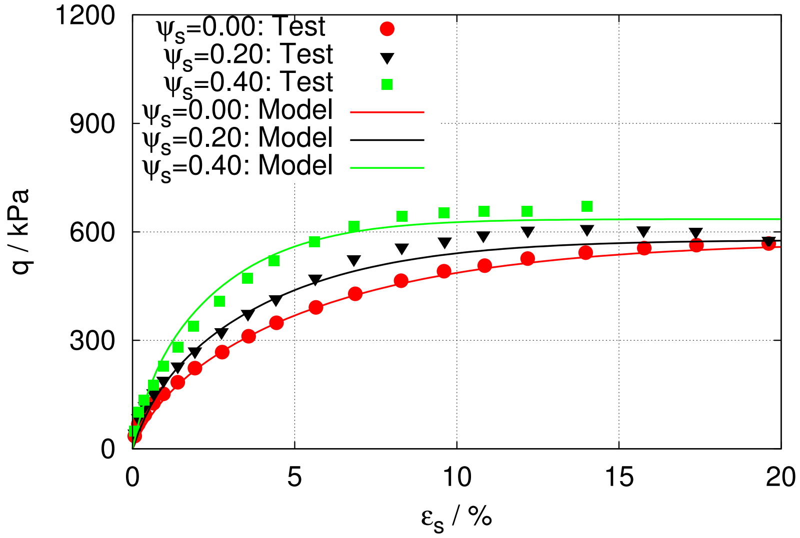

(b) ψ_a=0.20, 0.40

Figure 5: Experimental stress-strain data and numerical simulations HTP series (Natural gap-graded soils)

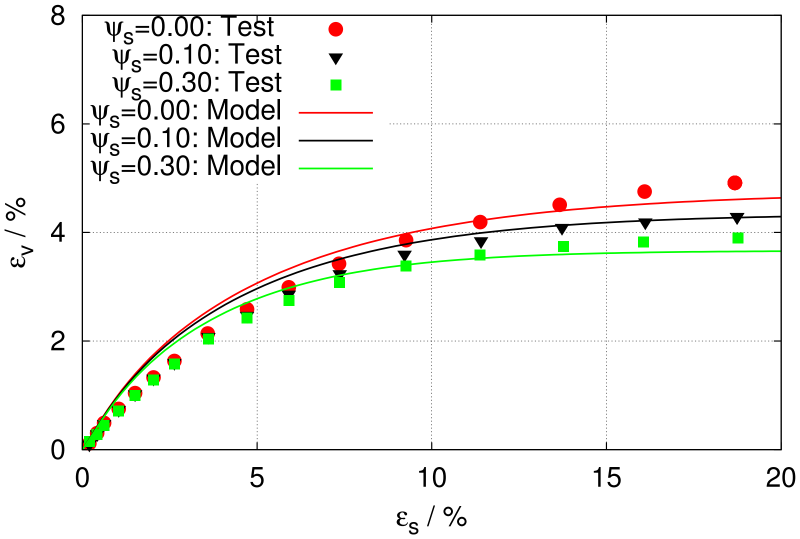

(a) ψ_a=0.10, 0.30

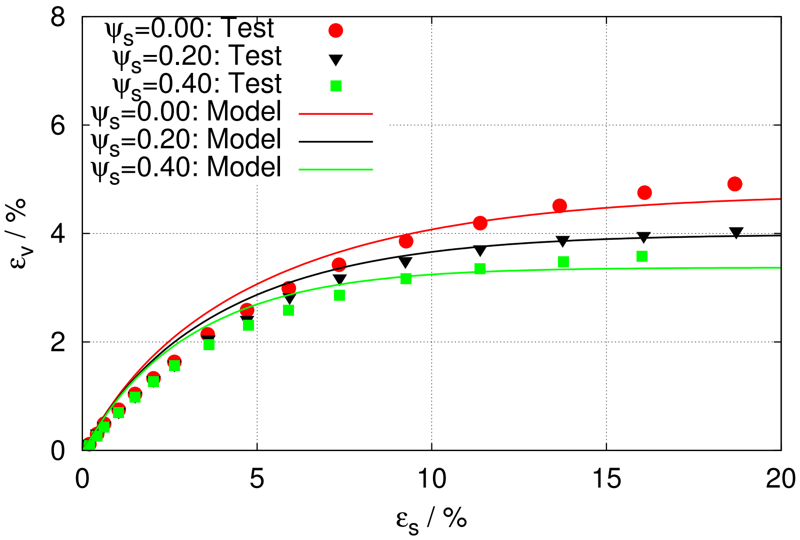

(b) ψ_a=0.20, 0.40

Figure 6: Experimental volumetric strain and numerical simulations of HTP series (Natural gap-graded soils)

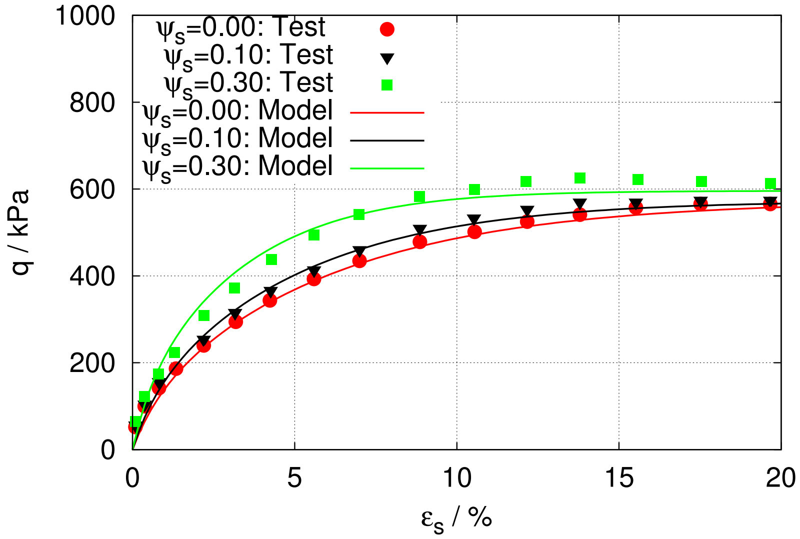

(a) ψ_a=0.10, 0.30

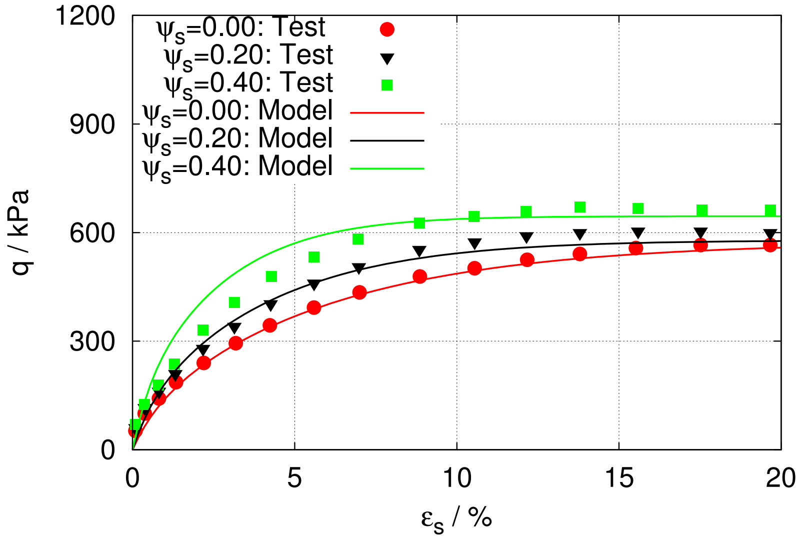

(b) ψ_a=0.20, 0.40

Figure 7: Experimental stress-strain data and numerical simulations HTP10 series (Natural gap-graded soils)

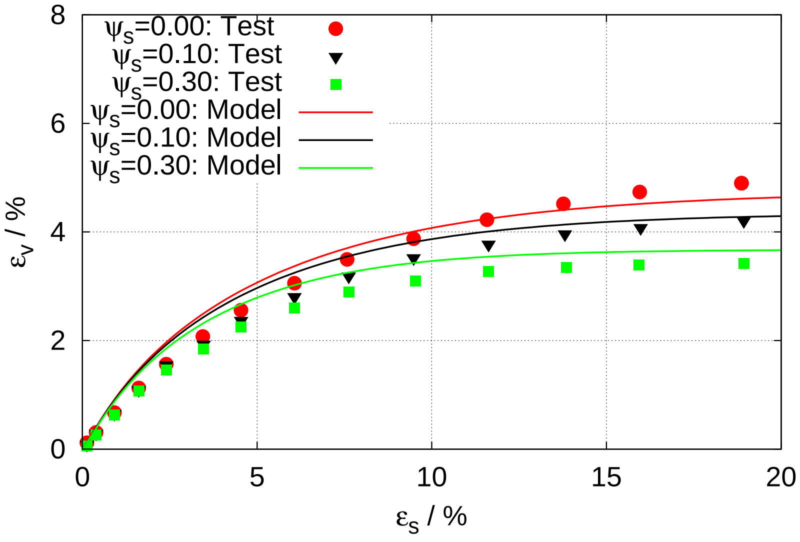

(a) ψ_a=0.10, 0.30

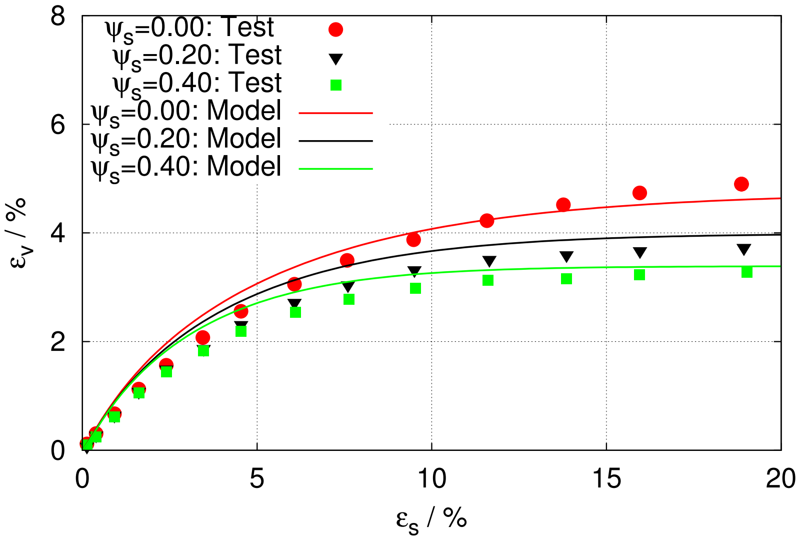

(b) ψ_a=0.20, 0.40

Figure 8: Experimental volumetric strain and numerical simulations of HTP10 series (Natural gap-graded soils)

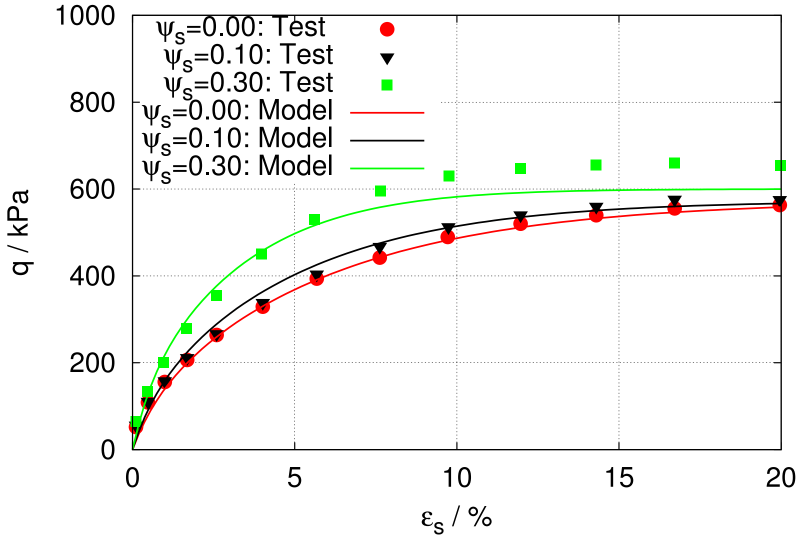

(a) ψ_a=0.10, 0.30

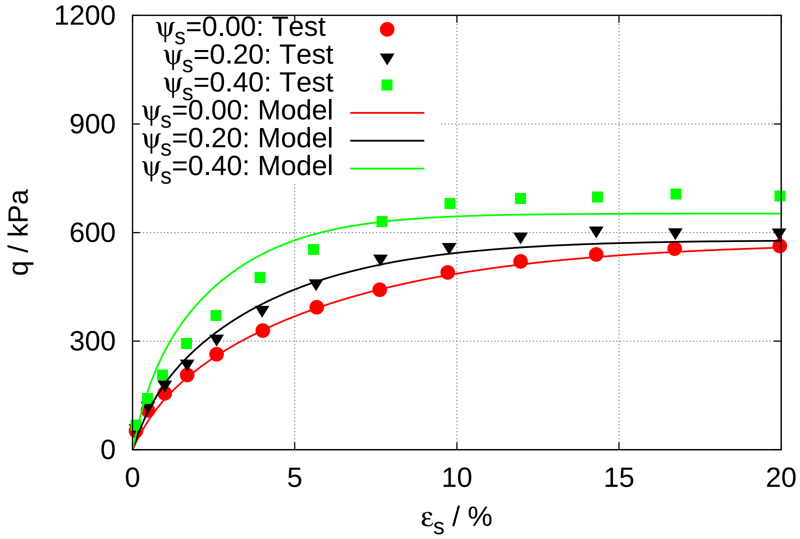

(b) ψ_a=0.20, 0.40

Figure 9: Experimental stress-strain data and numerical simulations HTP40 series (Natural gap-graded soils)

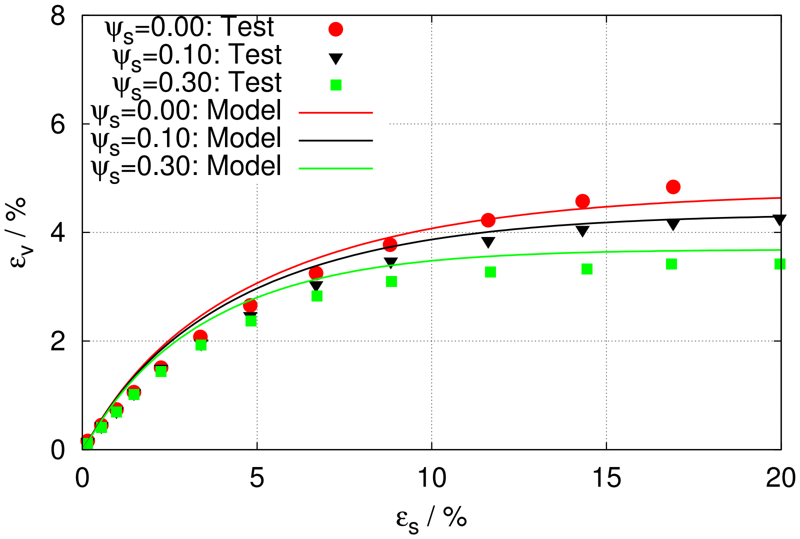

(a) ψ_a=0.10, 0.30

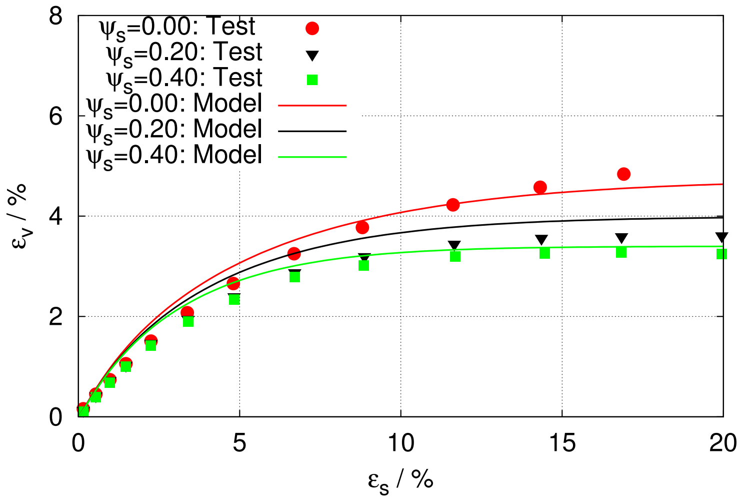

(b) ψ_a=0.20, 0.40

Figure 10: Experimental volumetric strain and numerical simulations of HTP40 series (Natural gap-graded soils)

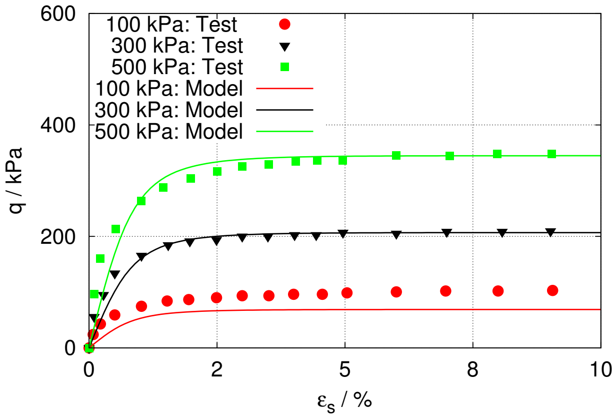

(a) ϕ_a=0.00

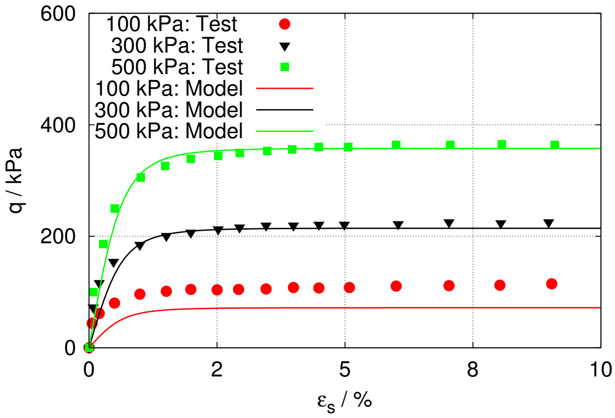

(b) ϕ_a=0.20

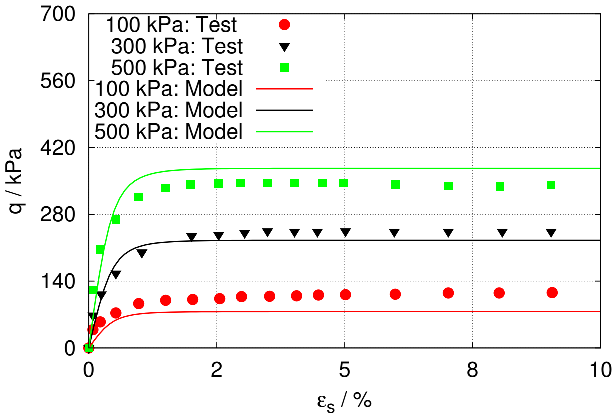

(c) ϕ_a=0.40

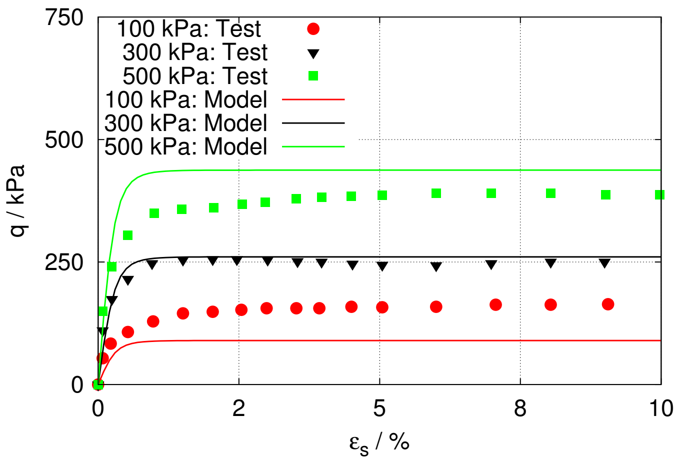

(d) ϕ_a=0.60

Figure 11: Experimental stress-strain data and numerical simulations (Kaolin clay-gravel mixtures)

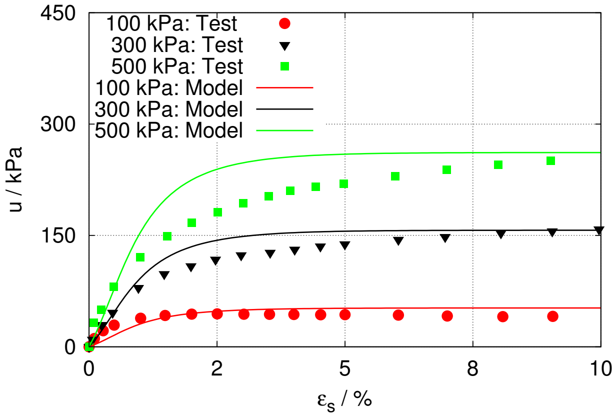

(a) ϕ_a=0.00

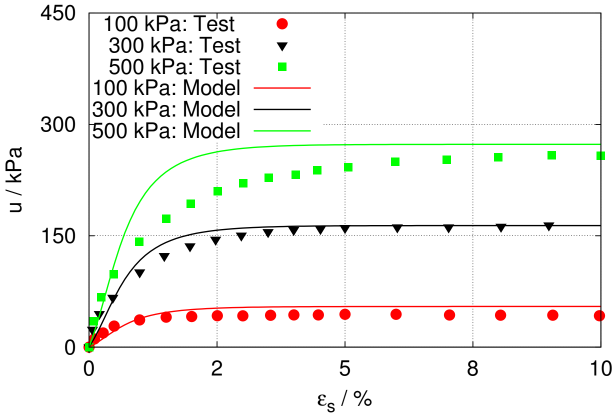

(b) ϕ_a=0.20

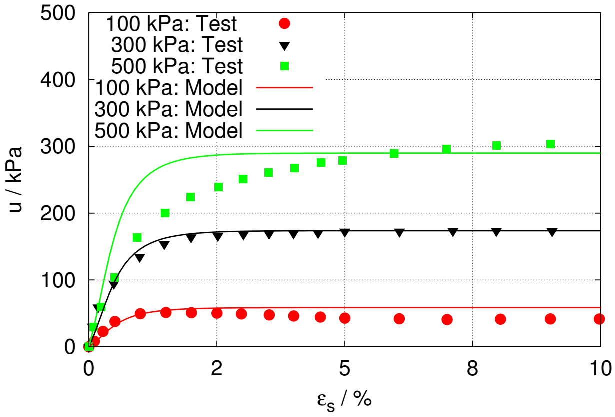

(c) ϕ_a=0.40

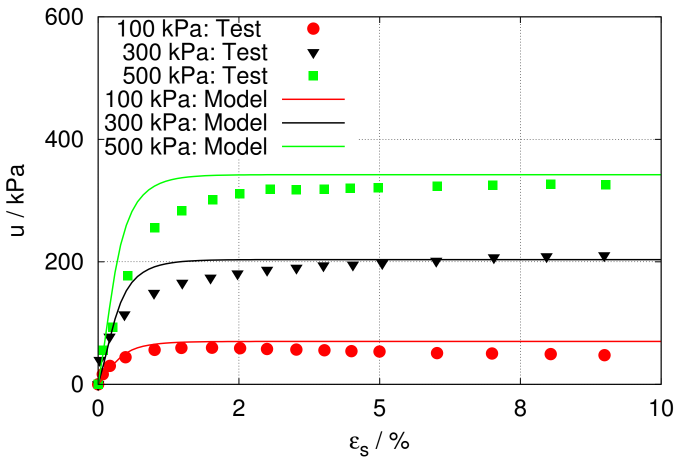

(d) ϕ_a=0.60

Figure 12: Experimental data of excess pore water pressure dissipation and numerical simulations (Kaolin clay-gravel mixtures)

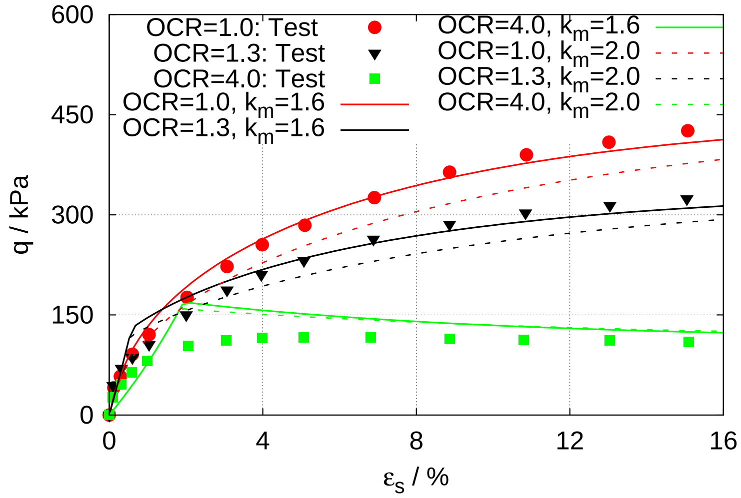

(a) ψ_a=0.00

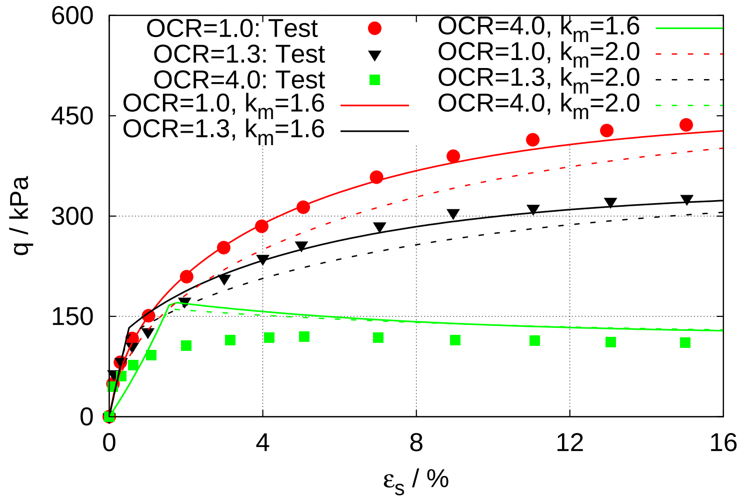

(b) ψ_a=0.30

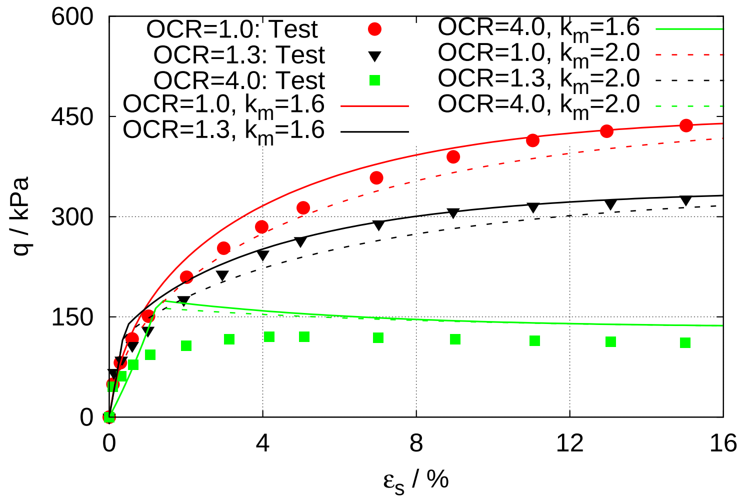

(c) ψ_a=0.50

Figure 13: Experimental stress-strain data and numerical simulations of drained triaxial test (Kaolin clay-sand mixtures)

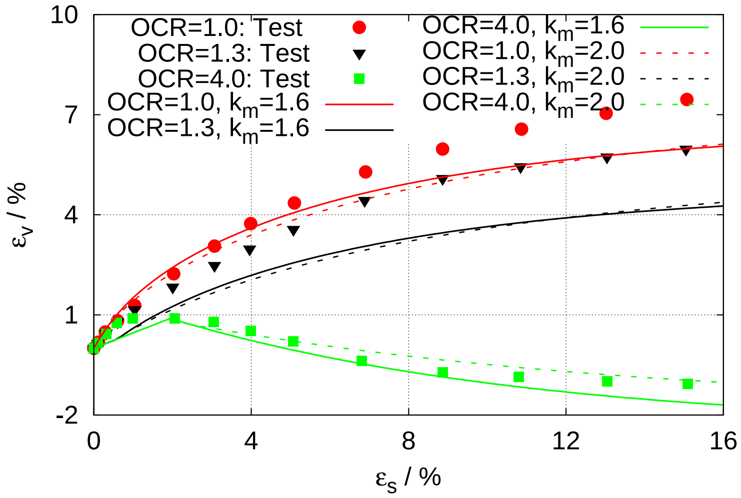

(a) ψ_a=0.00

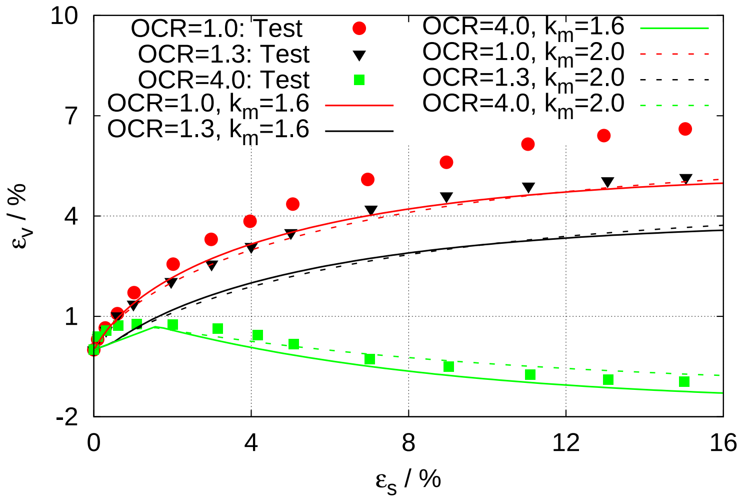

(b) ψ_a=0.30

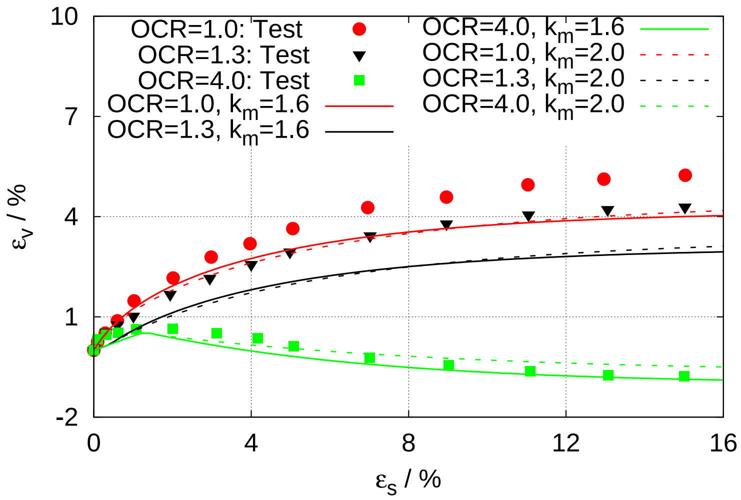

(c) ψ_a=0.50

Figure 14: Experimental volumetric strain and numerical simulations of drained triaxial test (Kaolin clay-sand mixtures)

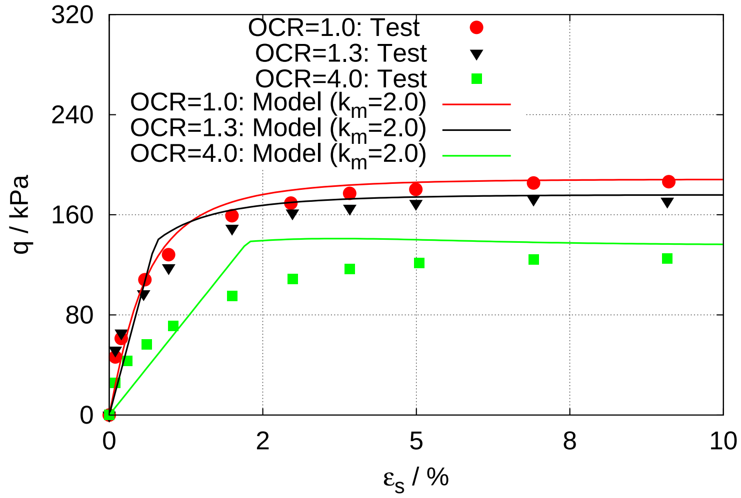

(a) ψ_a=0.00

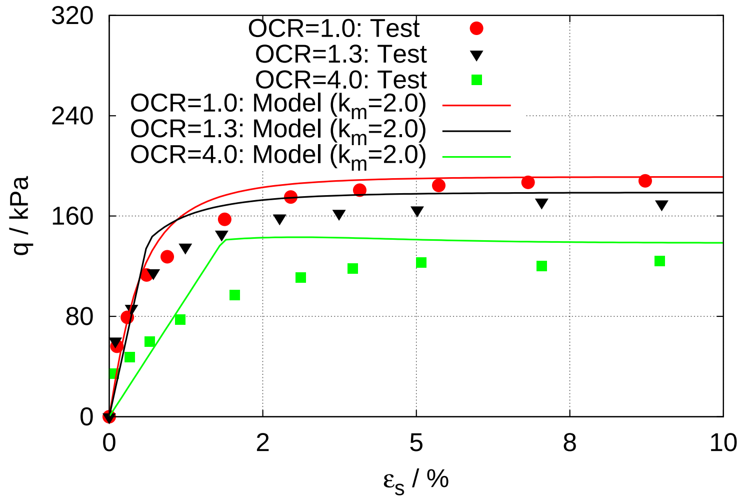

(b) ψ_a=0.30

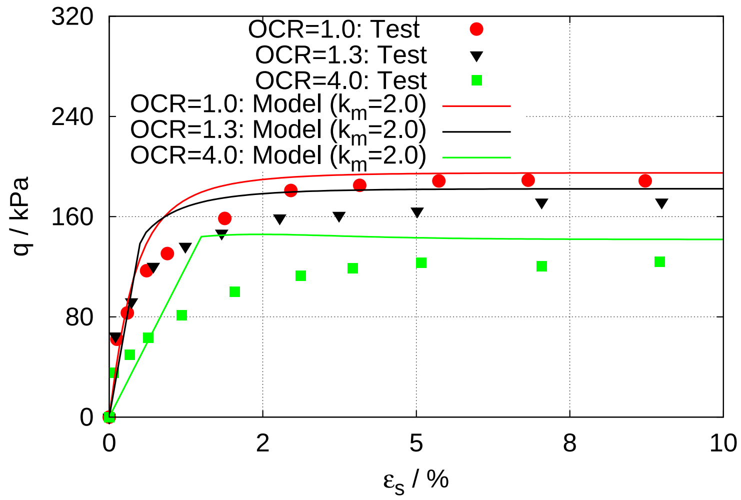

(c) ψ_a=0.50

Figure 15: Experimental stress-strain data and numerical simulations of undrained triaxial test (Kaolin clay-sand mixtures)

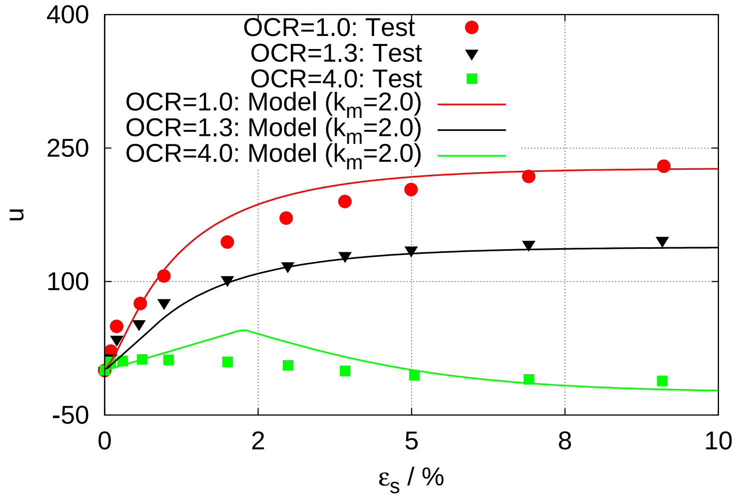

(a) ψ_a=0.00

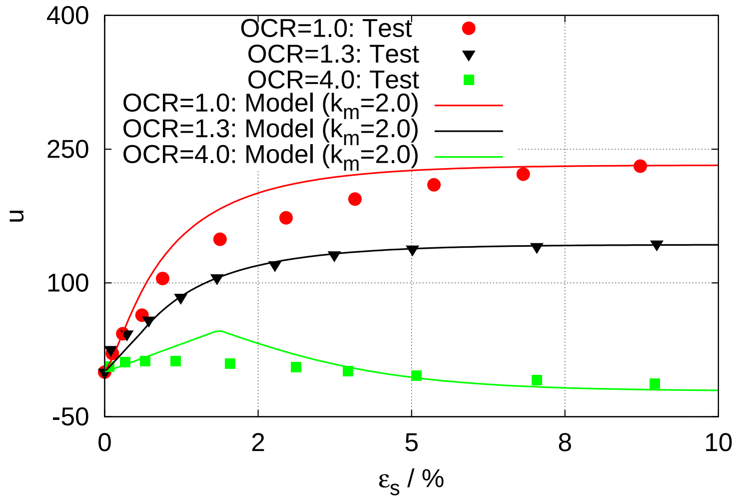

(b) ψ_a=0.30

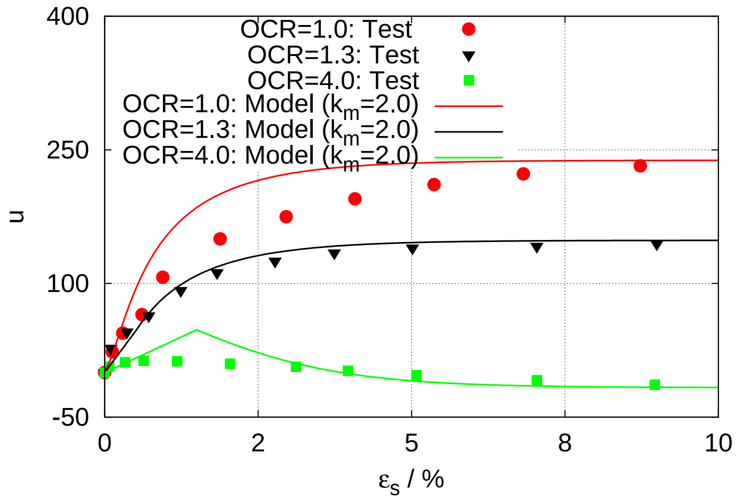

(c) ψ_a=0.50

Figure 16: Experimental data of excess pore water pressure dissipation and numerical simulations of undrained triaxial test (Kaolin clay-sand mixtures)